CELL BIOLOGY

10.1126/sciadv.1500603

Regulated lysosomal exocytosis mediates cancer progression

Eda Machado,[1]* Shai White-Gilbertson,[1]*† Diantha van de Vlekkert,[1]‡ Laura Janke,[2]‡ Simon Moshiach,[1] Yvan Campos,[1] David Finkelstein,[3] Elida Gomero,[1] Rosario Mosca,[1] Xiaohui Qiu,[1] Christopher L. Morton,[4] Ida Annunziata,[1] Alessandra d'Azzo[1]§

Understanding how tumor cells transition to an invasive and drug-resistant phenotype is central to cancer biology, but the mechanisms underlying this transition remain unclear. We show that sarcomas gain these malignant traits by inducing lysosomal exocytosis, a ubiquitous physiological process. During lysosomal exocytosis, the movement of exocytic lysosomes along the cytoskeleton and their docking at the plasma membrane involve LAMP1, a sialylated membrane glycoprotein and target of the sialidase NEU1. Cleavage of LAMP1 sialic acids by NEU1 limits the extent of lysosomal exocytosis. We found that by down-regulation of NEU1 and accumulation of oversialylated LAMP1, tumor cells exacerbate lysosomal exocytosis of soluble hydrolases and exosomes. This facilitates matrix invasion and propagation of invasive signals, and purging of lysosomotropic chemotherapeutics. In *Arf*$^{-/-}$ mice, *Neu1* haploinsufficiency fostered the development of invasive, pleomorphic sarcomas, expressing epithelial and mesenchymal markers, and lysosomal exocytosis effectors, LAMP1 and Myosin-11. These features are analogous to those of metastatic, pleomorphic human sarcomas, where low NEU1 levels correlate with high expression of lysosomal exocytosis markers. In a therapeutic proof of principle, we demonstrate that inhibiting lysosomal exocytosis reversed invasiveness and chemoresistance in aggressive sarcoma cells. Thus, we reveal that this unconventional, lysosome-regulated pathway plays a primary role in tumor progression and chemoresistance.

INTRODUCTION

Lysosomal exocytosis is a calcium-regulated process that entails recruiting a pool of lysosomes to the cytoskeletal network for transport to and docking at the plasma membrane (PM). Upon calcium influx, docked lysosomes fuse with the PM and extracellularly release their luminal contents (*1*, *2*). A key mediator of the docking step of the pathway is LAMP1, an integral lysosomal membrane protein whose highly glycosylated and sialylated luminal domain is a substrate of the lysosomal sialidase NEU1 (*1*, *3*). Sialidases hydrolyze terminal sialic acids on sialoglycoconjugates, and NEU1 is the most widely expressed of the four mammalian sialidases (*4*).

NEU1 deficiency leads to accumulation of NEU1 substrates, extensive lysosomal vacuolization, and tissue/organ degeneration, as evidenced in the neurosomatic, pediatric disease sialidosis (*5*, *6*). NEU1 limits lysosomal exocytosis by processing LAMP1 sialic acids, thereby shortening its half-life (*1*). If NEU1 is deficient or defective, LAMP1 remains oversialylated and accumulates at the lysosomal membrane. The latter feature renders lysosomes prone to tether and dock at the PM, ready to engage in lysosomal exocytosis (*1*). The end result is excessive exocytosis of lysosomal contents into the extracellular space with deleterious consequences for PM and extracellular matrix (ECM) integrity. Thus, NEU1 is the first and so far the only negative regulator of lysosomal exocytosis, and LAMP1 is an active component of this process (*1*). In the *Neu1*$^{-/-}$ mouse model of sialidosis (*6*), excessive lysosomal exocytosis underlies many of the disease's pathologic manifestations (*1*, *7*, *8*). Specifically, in muscle connective tissue, increased lysosomal exocytosis causes both hyperproliferation of myofibroblasts and excessive deposition and processing of the ECM. The aberrantly expanded connective tissues gradually infiltrate/invade the muscle bed, ultimately leading to degeneration of myofibers (*7*). Together, these phenotypic changes resemble those of invasive tumor cells; hence, we wanted to test the hypothesis that deregulated lysosomal exocytosis promotes cancer progression.

The foremost clinical hurdles in cancer treatment are metastatic disease and chemotherapy resistance, and the identification of molecular pathways mediating these processes is the focus of intensive research in the field. Soft tissue sarcomas are some of the most aggressive, untreatable cancers. Histologic subtypes have been identified, many of which are highly heterogeneous and thus difficult to diagnose and treat. This is especially true for pleomorphic sarcomas, which are characterized by high genomic instability, resulting in complex karyotypes (*9*, *10*). Mixed, undefined cell types that are generally negative for common tumor markers comprise pleomorphic sarcomas; hence, diagnosis is often by exclusion. Giant, rhabdoid, eosin^{+} cells distinguish the most malignant, high-grade, metastatic disease (*11*–*13*).

Therapeutic regimens for sarcomas currently include inhibitors of tyrosine kinases, vascular endothelial growth factor (VEGF), or mammalian target of rapamycin (mTOR) and monoclonal antibodies, which are frequently combined with chemotherapeutics (for example, doxorubicin) (*14*). However, these regimens mostly do not prevent relapse in patients with advanced disease (*14*, *15*). An event generally overlooked is the ineffective intracellular delivery of chemotherapeutics,

[1]Department of Genetics, St. Jude Children's Research Hospital, 262 Danny Thomas Place, Memphis, TN 38105, USA. [2]Department of Veterinary Pathology, St. Jude Children's Research Hospital, Memphis, TN 38105, USA. [3]Department of Computational Biology, St. Jude Children's Research Hospital, Memphis, TN 38105, USA. [4]Department of Surgery, St. Jude Children's Research Hospital, Memphis, TN 38105, USA.
*These authors contributed equally to this work.
†Present address: Hollings Cancer Center Tumor Registry, Medical University of South Carolina, Charleston, SC 29403, USA.
‡These authors contributed equally to this work.
§Corresponding author. E-mail: sandra.dazzo@stjude.org

which may affect the response to treatment. Anthracycline and vinca alkaloid drugs are preferentially sequestered in the acidic lysosomes because of their lipophilic, weak base characteristics, thereby diminishing their cytotoxicity (*16*).

A recognized determinant of the neoplastic process is the composition of glycans on cell surface receptors and adhesion molecules that influences their biochemical and functional properties (*17*, *18*). This is particularly the case for sialic acids, bulky, charged sugar residues at the termini of glycan chains, whose aberrant processing affects cell-cell and cell-ECM interactions, cell migration and adhesion, intracellular signaling, and metastatic potential (*17*, *18*). Thus, it is not surprising that all four mammalian sialidases have been implicated in tumor growth and spread (*19*, *20*). Of particular relevance are the studies demonstrating that overexpression of *NEU1* in metastatic colon carcinoma cells reduces liver metastasis in mice and inhibits cell migration and invasion in vitro (*21*). The authors attributed these effects to NEU1-mediated processing of sialic acids on β_4 integrin and consequent attenuation of extracellular signal–regulated kinase 1/2 (ERK1/2) signaling pathways (*19*, *21*). Although these findings underscore the importance of NEU1 in cancer progression, they do not explain how cancer cells acquire the ability to migrate.

Here, we provide evidence that sarcomas exploit excessive lysosomal exocytosis of hydrolytic enzymes and exosomes downstream of NEU1 down-regulation to degrade/remodel the ECM and migrate/invade adjacent tissue. Simultaneously, exacerbation of lysosomal exocytosis enables tumor cells to efflux lysosomotropic chemotherapeutics. Thus, sarcomas adopt this process to progress to an aggressive, malignant phenotype. The identification of this NEU1-regulated pathway in aggressive sarcomas offers new diagnostic and therapeutic opportunities for these untreatable cancers.

RESULTS

Neu1$^{+/-}$*/Arf*$^{-/-}$ mice develop aggressive sarcomas

To investigate the contribution of NEU1-regulated lysosomal exocytosis in cancer, we compared the effects of low-*Neu1* expression in tumors in *Neu1*$^{+/-}$*/Arf*$^{-/-}$ mice with those in *Neu1*$^{+/+}$*/Arf*$^{-/-}$ mice (*22*). Even though the range of tumors was similar in the two experimental groups, distinct skewing toward the development of highly aggressive sarcomas occurred almost exclusively in the *Neu1*$^{+/-}$*/Arf*$^{-/-}$ mice (Fig. 1, A to C, and table S1). On the basis of their morphology, immunoreactivity to canonical tumor markers, and invasiveness, these sarcomas were categorized into two main subgroups: pleomorphic sarcomas that developed in the extremities, retroperitoneum, and lower back and nonpleomorphic sarcomas (Fig. 1, A and B).

Morphologically, the pleomorphic sarcomas were remarkably similar to the corresponding human tumors, in that they contained highly heterogeneous cell types, including spindle, epitheliod, and giant rhabdoid cells (Fig. 1E). Rhabdoid cells are characteristic of high-grade, human pleomorphic sarcomas (*12*, *23*). On the basis of their immunoreactivity toward a large panel of markers (table S2), these tumors were further classified as UPS, P-SSMD, P-LMS, and P-MPNST (Fig. 1, A and B). They were positive for mesenchymal and epithelial markers [for example, pan-cytokeratin, vimentin, smooth muscle actin, and smooth muscle myosin heavy chain (Myosin-11)] and for the epithelial-mesenchymal transition (EMT) inducer transforming growth factor β (TGFβ) (fig. S1). Like human tumors, most (65%) pleomorphic sarcomas in mice invaded the fascia/basement membranes and grew rapidly (Fig. 1C). The nonpleomorphic sarcoma group included, besides the tumor types listed above, OS, RMS, and SNOS (Fig. 1B). In some *Neu1*$^{+/-}$*/Arf*$^{-/-}$ mice, sarcomas developed concurrently with other malignancies (for example, hematologic tumors and carcinomas).

Immunostaining of *Neu1*$^{+/-}$*/Arf*$^{-/-}$ sarcomas for Neu1 and Lamp1 revealed that Neu1 expression was low or undetectable in most cases and inversely associated with high-Lamp1 expression (Fig. 1, D and E). This was particularly evident in the rhabdoid cells of pleomorphic sarcomas (Fig. 1E), where opposing levels of Neu1 and Lamp1 were predictive of enhanced lysosomal exocytosis. To test this further, we established primary cells from various types of sarcomas resected from *Neu1*$^{+/-}$*/Arf*$^{-/-}$ mice. Compared to wild-type cells, tumor cells had lower Neu1 activity and higher levels of high–molecular weight Lamp1, which was likely due to oversialylation (Fig. 1, F and G) (*1*). We quantified the extent of lysosomal exocytosis in these cell lines by measuring the activity of the lysosomal glycosidase β-hexosaminidase (β-Hex) released into the culture medium (*1*, *2*). All three primary cell lines showed substantially more β-Hex activity, indicating enhanced lysosomal exocytosis (Fig. 1H).

Inverse expression of NEU1 and LAMP1 is common in human sarcomas

We next tested the levels of NEU1 and LAMP1 in human sarcomas by using tissue microarrays (TMAs) derived from tumors of smooth (LMS) or skeletal muscle (RMS) origin. The LMS arrays included tumors from different locations, clinical stage, and grade. NEU1 expression was low or undetectable in most cases, and LAMP1 expression was robust (Fig. 2, A and B). Notably, NEU1 was absent in two of the three stage III cases of LMS, one of which was pleomorphic. The RMS arrays included embryonal, alveolar, spindle cell, and pleomorphic types. Also, in these tumors, NEU1 expression was decreased in most cases, concomitantly with increased LAMP1 expression (Fig. 2, C and D). Most (73%) stage III/IV cases expressed very low or no NEU1. These results were confirmed in 14 patient-derived RMS xenografts (*24*) generated from primary or recurrent tumors (Fig. 2, E and F). RMS with low NEU1 showed high LAMP1 levels (Fig. 2E). The best example of this inverse expression pattern was seen in a case, for which we had xenografts of the primary tumor and the relapse (Fig. 2F). NEU1 was detected in the primary tumor but not in the relapse, whereas LAMP1 levels were higher in the relapse (Fig. 2F). These analyses suggest that inverse expression of NEU1 and LAMP1 consistently associates with the most malignant forms of soft tissue sarcomas.

Human RMS cells with low NEU1 and high LAMP1 have excessive lysosomal exocytosis

To dissect the low-NEU1–high-LAMP1 mechanism controlling lysosomal exocytosis in sarcomas, we used two well-characterized RMS cell lines, RH41 and RH30 (*25*), that have divergent NEU1 expression levels (Fig. 3, A to C, and fig. S2A). Low NEU1 activity in RH30 cells (Fig. 3B) led to increased LAMP1 in these cells compared to that in RH41 cells (Fig. 3C and fig. S2B). Using affinity chromatography with α2,6- or α2,3-sialic acid–binding lectins, we also demonstrated that LAMP1 accumulated in an oversialylated state especially in RH30 cells (Fig. 3D). Given that accumulation of oversialylated LAMP1 at the lysosomal membrane was shown to increase the number of lysosomes poised to tether to and dock at the PM (*1*, *7*, *8*, *26*), we compared the number and intracellular location of lysosomes in both RMS cell lines.

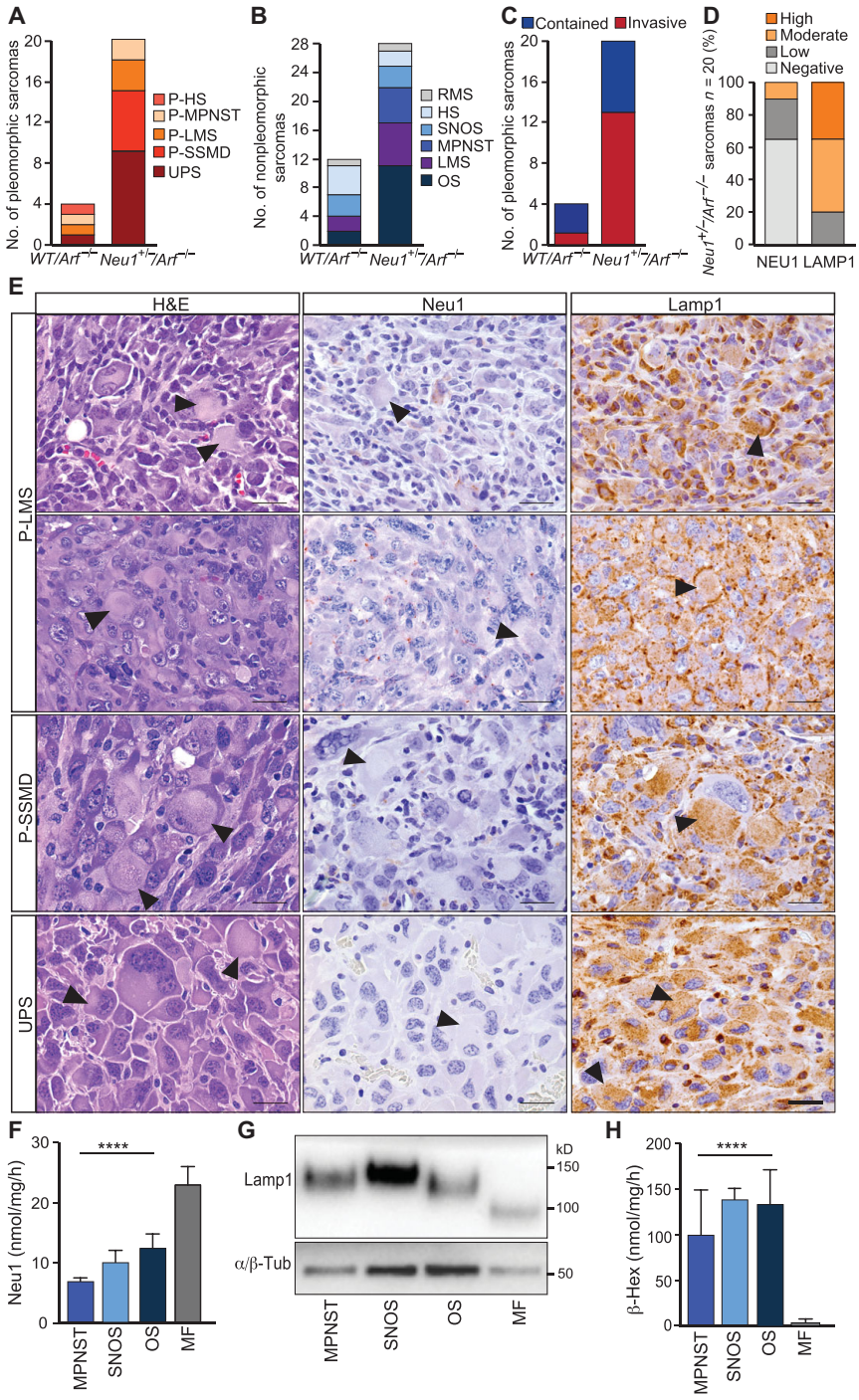

Fig. 1. Pleomorphic sarcomas are prevalent in *Neu1*$^{+/-}$/*Arf*$^{-/-}$ mice. (**A** and **B**) Numbers and types of pleomorphic (A) and nonpleomorphic (B) sarcomas that developed in *WT/Arf*$^{-/-}$ and *Neu1*$^{+/-}$/*Arf*$^{-/-}$ mice. (**C**) Number of contained versus invasive pleomorphic sarcomas. (**D**) Quantification of NEU1 and LAMP1 expression levels in 20 sarcomas from *Neu1*$^{+/-}$/*Arf*$^{-/-}$ mice. (**E**) Representative images of four pleomorphic sarcomas from *Neu1*$^{+/-}$/*Arf*$^{-/-}$ mice with epithelioid/rhabdoid and spindle cells, as shown by hematoxylin and eosin (H&E) staining, and absent or low Neu1 and strong Lamp1 immunostaining. Examples of rhabdoid cells are marked with arrowheads. Scale bar, 25 μm. (**F**) Neu1 activity in cells isolated from *Neu1*$^{+/-}$/*Arf*$^{-/-}$ sarcomas compared with that in differentiated myofibers (MF) from *WT/Arf*$^{-/-}$ mice ($n = 5$). (**G**) Lamp1 levels in cells isolated from *Neu1*$^{+/-}$/*Arf*$^{-/-}$ sarcomas compared with that in *WT/Arf*$^{-/-}$ MF. α/β-Tubulin was used as the loading control. (**H**) β-Hex activity assayed in the culture medium of *Neu1*$^{+/-}$/*Arf*$^{-/-}$ sarcomas cells compared with that of *WT/Arf*$^{-/-}$ MF, as a measure of lysosomal exocytosis ($n = 5$). OS, osteosarcoma; P-HS, pleomorphic hemangiosarcoma; P-LMS, pleomorphic leiomyosarcoma; P-MPNST, pleomorphic malignant peripheral nerve sheath tumor; P-SSMD, pleomorphic sarcoma with smooth muscle differentiation; RMS, rhabdomyosarcoma; SNOS, sarcoma non-otherwise specified; UPS, undifferentiated pleomorphic sarcoma. Data are means ± SD. ****$P < 0.0001$, Student's *t* test for unpaired samples.

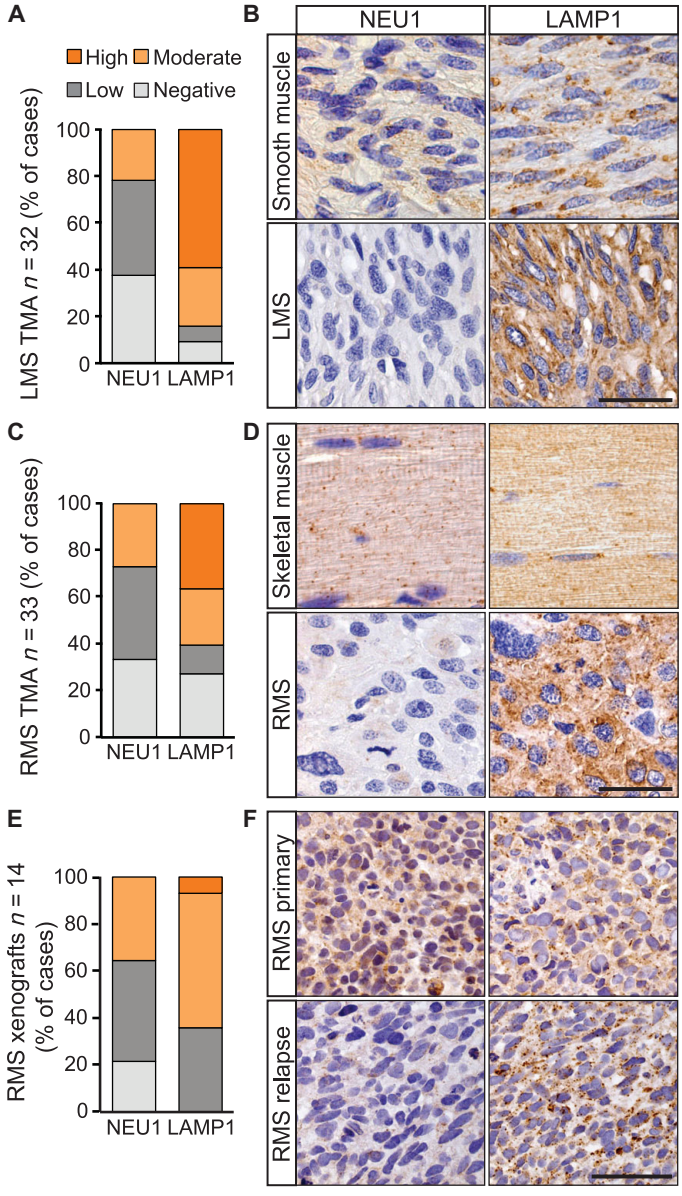

Fig. 2. NEU1 and LAMP1 expression levels vary inversely in LMS and RMS. (**A**) Quantification of NEU1 and LAMP1 expression levels in 32 LMS tissue arrays. (**B**) Representative images of LMS and healthy tissues immunostained for NEU1 and LAMP1. (**C**) Quantification of NEU1 and LAMP1 expression levels in 33 RMS tissue arrays. (**D**) Representative images of RMS and healthy tissues immunostained for NEU1 and LAMP1. (**E**) Quantification of NEU1 and LAMP1 expression levels in 14 patient-derived RMS xenografts. (**F**) Representative images of primary and relapse RMS xenografts from the same patient immunostained for NEU1 and LAMP1. Scale bars, 25 μm.

We first assessed the spatial positioning of lysosomes by confocal microscopy; in RH30 cells, lysosomes were primarily positioned at the cell periphery and continuously dispatched from the cell center outward (Fig. 3E, movie S2, and fig. S2C). In RH41 cells, most lysosomes resided in the perinuclear space (Fig. 3E, movie S1, and fig. S2C). Using live total internal reflection fluorescence (TIRF) imaging of LysoTracker-labeled lysosomes, we showed that RH30 cells had a significantly higher number of lysosomes tethered to or docked at the PM compared to RH41 cells (Fig. 3F, movies S3 and S4, and fig. S2D). These results, combined with the detection of increased LAMP1 at the PM (fig. S2E), were suggestive of enhanced lysosomal exocytosis in RH30 cells. To confirm this assumption, we first measured the levels of fluorescence-labeled dextran effluxed by RH41 and RH30 cells. Both cell lines internalized this compound equally well (fig. S2, G and H), but RH30 cells released it extracellularly in greater amounts than did RH41 cells (fig. S2F). Unequivocal proof that lysosomal exocytosis was indeed exacerbated in RH30 cells compared to RH41 cells was obtained by measuring β-Hex activity in the medium (Fig. 3G). Moreover, considering the attention given recently to the role of exosomes in cancer progression (*27*–*31*), we wanted to test whether enhanced lysosomal exocytosis in low-NEU1–expressing cells would promote increased release of exosomes. We detected a significantly higher amount of exosomes in the medium of RH30 cells than in that of RH41 cells (Fig. 3H). We established that these released microvesicles were bona fide exosomes by probing Western blots of the exosome purified preparations with canonical exosomal markers (Fig. 3I) (*32*).

The involvement of LAMP1 in promoting the movement of lysosomes to the cell periphery and consequently increased lysosomal exocytosis in the RH30 cells was demonstrated by silencing *LAMP1* ($RH30^{shLAMP1}$) (Fig. 3J). This resulted in fewer $LysoTracker^{+}$ lysosomes detected by TIRF imaging in the vicinity of the PM (Fig. 3K) and, consequently, in decreased β-Hex activity in the medium and reduced amounts of exocytosed exosomes (Fig. 3, H and L). Knocking down NEU1 in RH41 ($RH41^{shNEU1}$) or overexpressing NEU1 in RH30 ($RH30^{NEU1}$) also inversely modulated the extent of lysosomal exocytosis (fig. S2, I to P).

NEU1 down-regulation correlates with high *MYH11* expression in aggressive human sarcomas

To identify genes whose expression correlates with *NEU1* down-regulation and potentially synergizes with NEU1 to promote cancer progression, we queried a gene expression array of 309 sarcomas (*33*). Low *NEU1* was correlated with increased expression of four genes: *MYH11*, *CEP68*, *RABGAP1*, and *PGM5* (Fig. 4, A to C, and fig. S3, A to C). All these genes are expressed in skeletal or smooth muscle and are involved in actin cytoskeleton remodeling, cell division, vesicular trafficking, and centrosome cohesion (*34*–*37*). Although *CEP68*, *RABGAP1*, and *PGM5* showed inverse correlation with *NEU1*, they did not cluster in subgroups; instead, they followed a linear trend (fig. S3, A to C). The strongest correlation was between *NEU1* and *MYH11* (Pearson's $r = -0.488$), which formed a graphically separate subgroup (Fig. 4B). *MYH11* encodes the smooth muscle–specific motor Myosin-11 (*37*), which is often expressed in sarcomas with rhabdoid characteristics (for example, pleomorphic LMS, RMS, and UPS) (*12*, *13*, *23*) and is a biomarker of pleomorphic sarcomas (*13*). The *NEU1*/*MYH11* inverse correlation was particularly evident in metastatic LMS (Fig. 4C and fig. S3D). Correlation values were stronger ($P \leq 0.005$) when *NEU1* expression was scored against histologic subtype and location of the sarcomas (Fig. 4, D and E, and table S3); expression was lowest in 18 of 22 LMS of the retroperitoneum, which comprise the most aggressive, metastatic sarcomas (Fig. 4E and table S3).

To validate these expression profiles, we immunostained TMAs for Myosin-11. Within the LMS cohort, nine $Myosin\text{-}11^{+}$ tumors showed low NEU1 and high LAMP1. This was most evident in the stage IIIb pleomorphic LMS (Fig. 4F). The three pleomorphic cases of stage

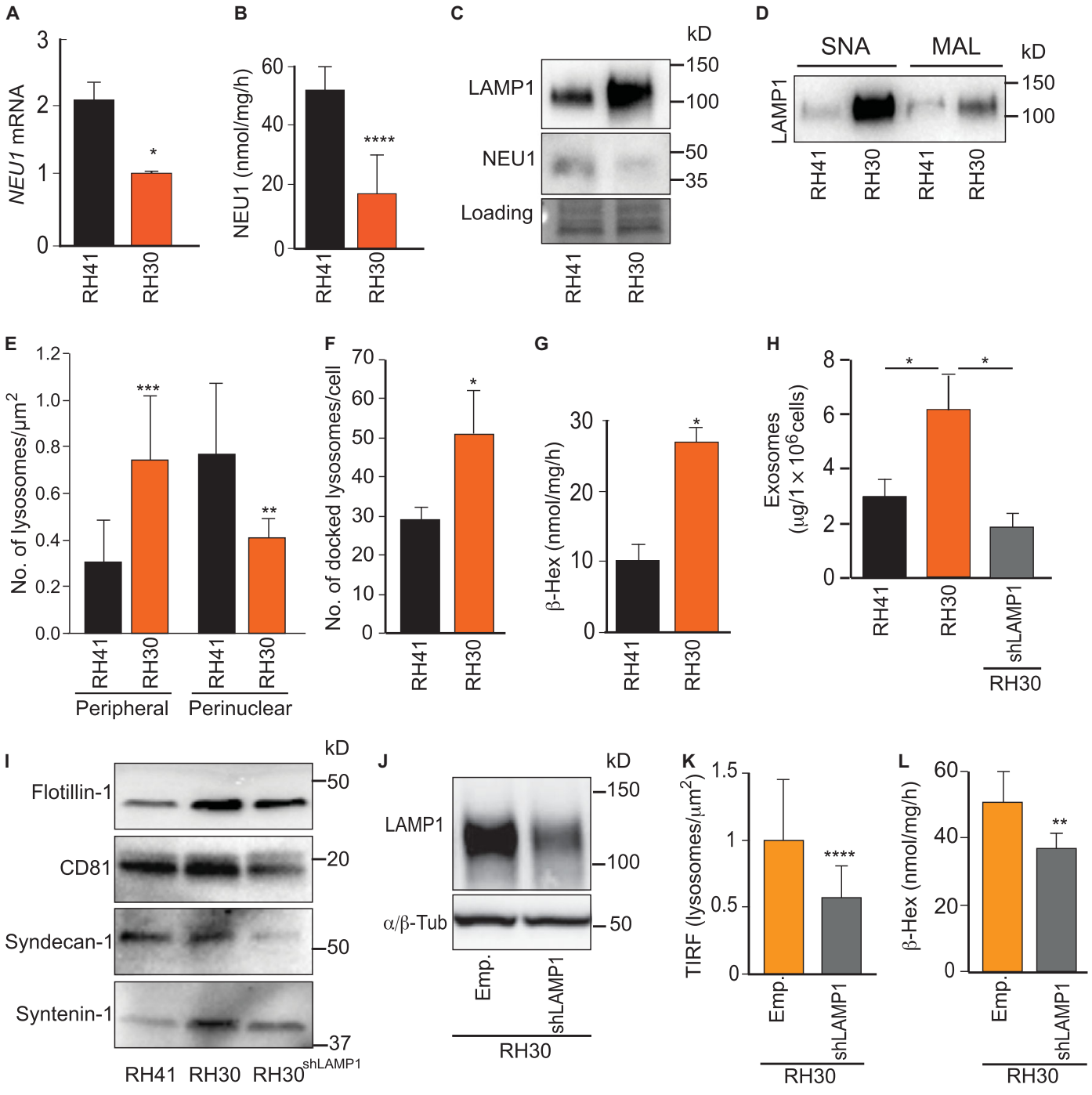

Fig. 3. Combined low NEU1 and high LAMP1 levels result in exacerbated lysosomal exocytosis in RMS cells. (**A**) Real-time quantitative polymerase chain reaction (RT-qPCR) of *NEU1* mRNA expression ($n = 4$). (**B**) NEU1 enzyme activity measured in RH41 and RH30 cells ($n = 4$). (**C**) Immunoblot of LAMP1 and NEU1 in RH41 and RH30 cells. (**D**) Sialic acid content detected on LAMP1 from RH41 and RH30 cells. The sialic acid–containing glycoproteins were purified through *Sambucus nigra* (SNA) and *Maackia amurensis* (MAL) columns, followed by LAMP1 immunoblotting. (**E**) Number of lysosomes distributed in the peripheral and perinuclear region of RH41 compared with RH30 cells ($n = 11$). (**F**) Number of lysosomes tethered to or docked at the PM of RH41 compared with RH30 cells quantified by live TIRF imaging ($n = 4$). (**G**) β-Hex activity assayed in the medium of RH41 and RH30 cell as a measure of lysosomal exocytosis ($n = 3$). (**H**) Quantification of exosomes released by RH41, RH30, and RH30^{shLAMP1} cells ($n = 4$). (**I**) Immunoblot of exosomal markers flotillin-1, CD81, syndecan-1, and syntenin-1 in exosome preparations purified from RH41, RH30, and RH30^{shLAMP1} medium. (**J**) Immunoblot of LAMP1 in RH30^{shLAMP1} cells and its empty vector control. (**K**) Number of LysoTracker^{+} lysosomes present in the evanescent field close to the PM of RH30^{shLAMP1} cells and their control cells quantified by TIRF microscopy ($n = 40$). (**L**) β-Hex activity assayed in the medium of RH30^{shLAMP1} cells and its empty vector control ($n = 5$). α/β-Tubulin was used as the loading control. Data are means ± SD or SE. *$P < 0.05$, **$P < 0.01$, ***$P < 0.001$, ****$P < 0.0001$, Student's t test for unpaired samples.

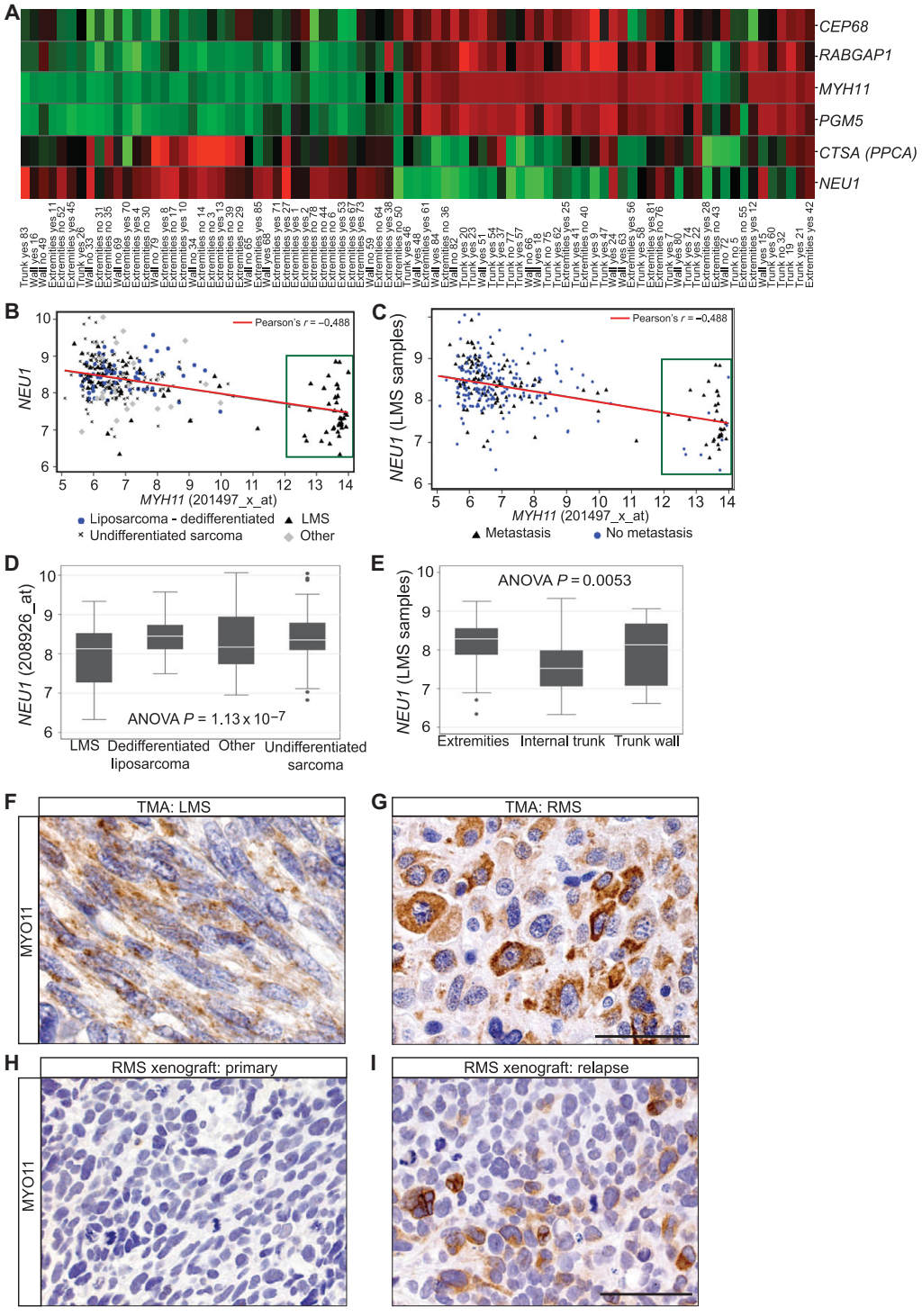

Fig. 4. *NEU1* gene expression in human sarcomas is inversely correlated with that of *MYH11*. (**A**) Heat map for *NEU1* positively or negatively correlated genes (*Z* score–normalized $\log_2$ expression) within different locations in LMS. Scale colors are graded from −2 (green), to 0 (black), to 2 (red). (**B**) Negative linear correlation (Pearson's $r = -0.488$) plot of *NEU1* $\log_2$ expression signals to *MYH11* $\log_2$ expression. The sarcoma class is distinctly split into a high-*MYH11*– and low-*MYH11*–expressing, with an isolated high-expressing class primarily composed of LMS (green box). (**C**) Correlation of *NEU1* $\log_2$ expression with *MYH11* (probe set 201497_x_at) $\log_2$ expression in LMS metastasis. A green box highlights the distinct subgroup of metastatic LMS expressing low *NEU1* and high *MYH11*. (**D**) Boxplot of *NEU1* expression depending on the histological type ($P = 1.13 \times 10^{-7}$) of sarcomas. (**E**) Boxplot of *NEU1* $\log_2$ expression within the LMS dependent on tumor location ($P = 0.0053$). Sarcoma gene set: GSE21050. (**F** and **G**) Representative image of a pleomorphic LMS (F) and a pleomorphic RMS (G) from human TMAs immunostained for Myosin-11 (MYO11). (**H**) Patient-derived RMS xenograft of a primary tumor and relapsed tumor from the same patient immunostained for Myosin-11. Scale bars, 25 μm.

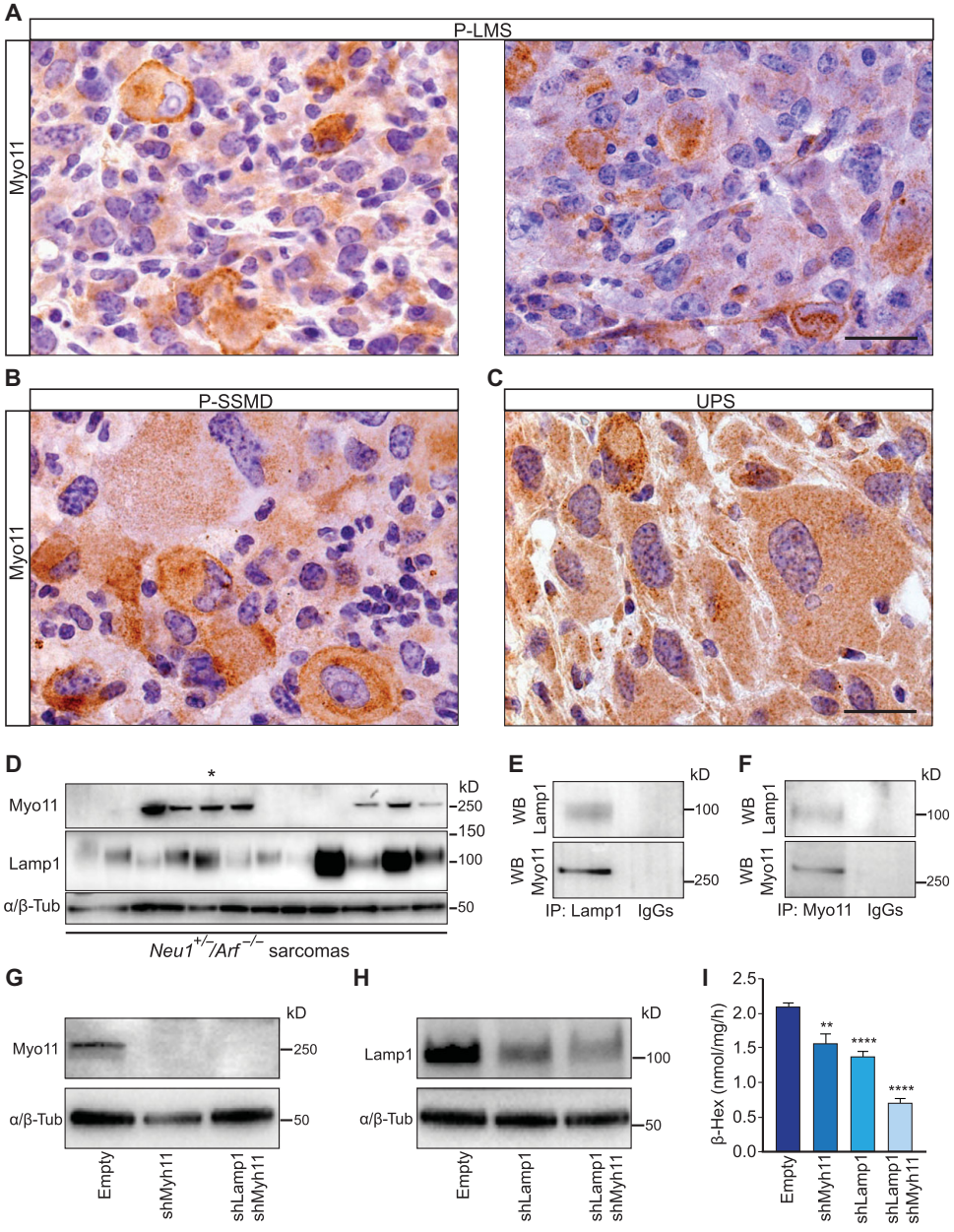

Fig. 5. Myosin-11 in sarcomas from *Neu1*$^{+/-}$/*Arf*$^{-/-}$ mice interacts with Lamp1 and contributes to lysosomal exocytosis. (**A** to **C**) Representative images of pleomorphic sarcomas from *Neu1*$^{+/-}$/*Arf*$^{-/-}$ mice with rhabdoid cells immunostained for Myosin-11. Scale bars, 25 μm. (**D**) Immunoblot of Myosin-11 and Lamp1 in primary cells isolated from different *Neu1*$^{+/-}$/*Arf*$^{-/-}$ sarcomas, that is, OS, MPNST, LMS, RMS, UPS, P-SSMD, and P-LMS. The sarcoma cells used for the coimmunoprecipitation assays and for silencing of *Myh11* and are indicated with "*." (**E**) Lamp1 antibody coimmunoprecipitated Myosin-11 from sarcoma cell extract. (**F**) Myosin-11 antibody coimmunoprecipitated Lamp1 from a cytoskeleton-enriched subcellular fraction of sarcoma cells. (**G**) Levels of Myosin-11 in sarcoma cells with silencing *Myh11* (shMyh11), and with silencing of both *Lamp1* and *Myh11* (shLamp1/shMyh11), compared with their empty vector controls. (**H**) Levels of Lamp1 in sarcoma cells with silenced *Lamp1* (shLamp1), and shLamp1/shMyh11, compared to their empty vector control. (**I**) β-Hex activity measured in the medium of shLamp1, shMyh11, or shLamp1/shMyh11 sarcoma cells compared to that assayed in their empty vector controls ($n = 4$). α/β-Tubulin was used as the loading control. Data are means ± SD. $^{**}P < 0.01$, $^{****}P < 0.0001$, Student's t test for unpaired samples.

IIa/IIIb RMS were Myosin-11$^+$, though Myosin-11 is usually not expressed in RMS (Fig. 4G). Again, the tumors showed decreased NEU1 and increased LAMP1 expression (Fig. 2, B and D). We also tested patient-derived RMS xenografts and demonstrated Myosin-11 immunoreactivity in three cases: two were relapses of Myosin-11$^-$ primary tumors (Fig. 4H). These findings indicate that in most of the highly malignant human sarcomas, the low-NEU1–high-LAMP1 pattern is associated with high Myosin-11 expression, suggesting that they synergistically promote an invasive/metastatic state.

In *Neu1*$^{+/-}$*/Arf*$^{-/-}$ mice, Myosin-11 interacts with Lamp1 and contributes to increased lysosomal exocytosis

We next measured Myosin-11 expression in pleomorphic and nonpleomorphic sarcomas in our *Neu1*$^{+/-}$*/Arf*$^{-/-}$ mouse model (Fig. 5, A to C). Myosin-11$^+$ staining was detected in most pleomorphic sarcomas with rhabdoid cells that also showed absent or low Neu1 and high Lamp1 (Figs. 1E and 5, A to C). As observed in human samples, the rhabdoid cells were highly Myosin-11$^+$. These results replicated those obtained in human sarcomas with rhabdoid features, making these mice a potential model of this type of sarcomas.

Because Myosin-11 expression correlated with high Lamp1 and low Neu1 (Figs. 2, A to D, and 4, B and C), we hypothesized that this motor myosin could directly or indirectly interact with Lamp1 and thus take part in the trafficking of lysosomes to the PM. To test this possibility, we cross-immunoprecipitated Myosin-11 and Lamp1 from *Neu1*$^{+/-}$*/Arf*$^{-/-}$ sarcoma cells that expressed high levels of both proteins (Fig. 5, D to F, and fig. S4, A to D). Cross-immunoprecipitation of the two endogenous proteins was performed using anti-LAMP1 or an anti–Myosin-11 antibody and visualized on Western blots (Fig. 5, E and F, and fig. S4, A to D). Anti–Myosin-11 antibody did not coimmunoprecipitate LAMP3 or CD63 (fig. S5, A and B). These results support the idea that Lamp1 specifically interacts with this motor myosin to facilitate lysosome trafficking to the cell periphery. Silencing *Myh11*, *Lamp1*, or the combination of the two in the same tumor cells lowered lysosomal exocytosis (Fig. 5, G to I), confirming that Myosin-11 and Lamp1 are both involved in the trafficking of lysosomes to the PM and consequently in lysosomal exocytosis.

Enhanced lysosomal exocytosis renders human sarcoma cells invasive and drug-resistant

We next tested the invasive capacity of RH41 and RH30 cells by seeding them onto *Neu1*$^{+/+}$ or *Neu1*$^{-/-}$ ex vivo peritoneal membranes. RH30 cells invaded the *Neu1*$^{+/+}$ peritoneum more readily than did RH41 cells, demonstrating their cell-autonomous ability to migrate through a basement membrane (Fig. 6A). Notably, the *Neu1*$^{-/-}$ peritoneum was more vulnerable to invasion by either cell line than was the *Neu1*$^{+/+}$ peritoneum (Fig. 6A). This was because Neu1 deficiency in the recipient peritoneum triggered increased release of hydrolytic enzymes that in part degraded its basement membrane components, that is, laminin and collagen IV (fig. S6A), and made it more permissive to cell invasion. Conversely, RH30^{shLAMP1} cells with attenuated lysosomal exocytosis had reduced ability to invade either peritonea (Fig. 6B). We confirmed that RH30 cells were more migratory than RH41 cells using an in vitro Transwell migration assay (Fig. 6C). Remarkably, we could enhance the migratory capacity of RH41 cells by culturing them in the presence of exosomes purified from the RH30 medium (Fig. 6C). This effect was not observed when RH41 cells were treated with RH30^{shLAMP1} exosomes (Fig. 6C). Thus, increased lysosomal exocytosis in tumor cells promotes invasion and degradation of the ECM, and may condition neighboring cells to become migratory via signals released by exocytosed exosomes.

These data were supported by the outcome of orthotopic xenografts generated in *Neu1*$^{+/+}$/NSG (nonobese diabetic *scid* γ) and *Neu1*$^{+/-}$/NSG mice using RH30 isogenic cells with low or high NEU1 expression. We modulated NEU1 levels by overexpressing its chaperone protective protein cathepsin A (PPCA). This approach stably increased endogenous NEU1 activity in vivo because of the long half-life of PPCA and its ability to stabilize NEU1 in lysosomes, as seen in CLFs of RH30^{PPCA} cells (Fig. 6, D and E, and fig. S6B) (*8*, *38*). Indeed, RH30^{PPCA} had higher NEU1 activity and lower LAMP1 levels compared to the unmodified cells, and they showed attenuated lysosomal exocytosis (Fig. 6F). RH30^{empty} orthotopic xenografts displayed the highest growth rate in *Neu1*$^{+/-}$/NSG mice (Fig. 6G). In contrast, RH30^{PPCA} xenografts grew at a rate similar to that of xenografts in *Neu1*$^{+/+}$/NSG mice (Fig. 6G). Thus, the combined effect of low NEU1 in tumor cells and the microenvironment created the most permissive setting for tumor growth and spread.

We hypothesized that increased lysosomal exocytosis affects the response of RMS cells to chemotherapeutics that are sequestered in lysosomes because of their weak base characteristics. We found that doxorubicin endogenous fluorescence colocalized, in part, with LysoTracker Green in RH41 and RH30 cells; however, in RH41 cells, doxorubicin-loaded lysosomes were mainly perinuclear, whereas in RH30 cells, they were scattered throughout the cytoplasm (fig. S7A). Live imaging of RH41 cells showed that doxorubicin trafficked rapidly to the nucleus, leading to apoptosis (movies S5 and S7); in RH30 cells, doxorubicin was primarily sequestered in lysosomes that were continuously shuttled to the cell surface and often clustered in cell protrusions, rendering the cells resistant to the drug (movies S6 and S8). Given that RH30 cells do not express the adenosine triphosphate–binding cassette (ABC) transporter P-glycoprotein-1 (Pgp) (fig. S7B) (*39*), we argued that increased lysosomal exocytosis would promote the efflux of lysosomal doxorubicin, providing a mechanism for chemoresistance. To confirm this assumption, we measured the levels of doxorubicin effluxed by RH41 and RH30 cells (Fig. 6H). Both cell lines internalized the drug equally well (Fig. 6J); however, quantification of the effluxed doxorubicin fluorescence showed that the drug was released in greater amounts from RH30 cells than from RH41 cells (Fig. 6H).

We unequivocally proved that the mechanism of drug efflux was lysosomal exocytosis, by using the pharmacologic compound verapamil. Being a calcium channel blocker, this clinically approved drug affects calcium intake by cells, and we hypothesized that this in turn would inhibit lysosomal exocytosis. Indeed, treatment of RH30 cells with verapamil drastically reduced the rate of exocytosed doxorubicin to the levels of that of RH41 cells (Fig. 6H and movie S9). Comparable reduction of drug efflux was also observed in RH30^{shLAMP1} cells treated with doxorubicin (Fig. 6I). Generating dose-response curves for doxorubicin treatment of the parental lines further validated these findings. RH30 cells were more resistant to doxorubicin than were RH41 cells, but became sensitive when treated with verapamil (Fig. 6K). Also, RH30^{shLAMP1} cells showed decreased viability when treated with doxorubicin, reiterating the importance of this effector of lysosomal exocytosis in chemoresistance (Fig. 6L).

Enhanced lysosomal exocytosis renders mouse sarcoma cells invasive and drug-resistant

We then tested the invasive and drug-resistant characteristics of our primary mouse cells isolated from *Neu1*$^{+/-}$*/Arf*$^{-/-}$ sarcomas that had

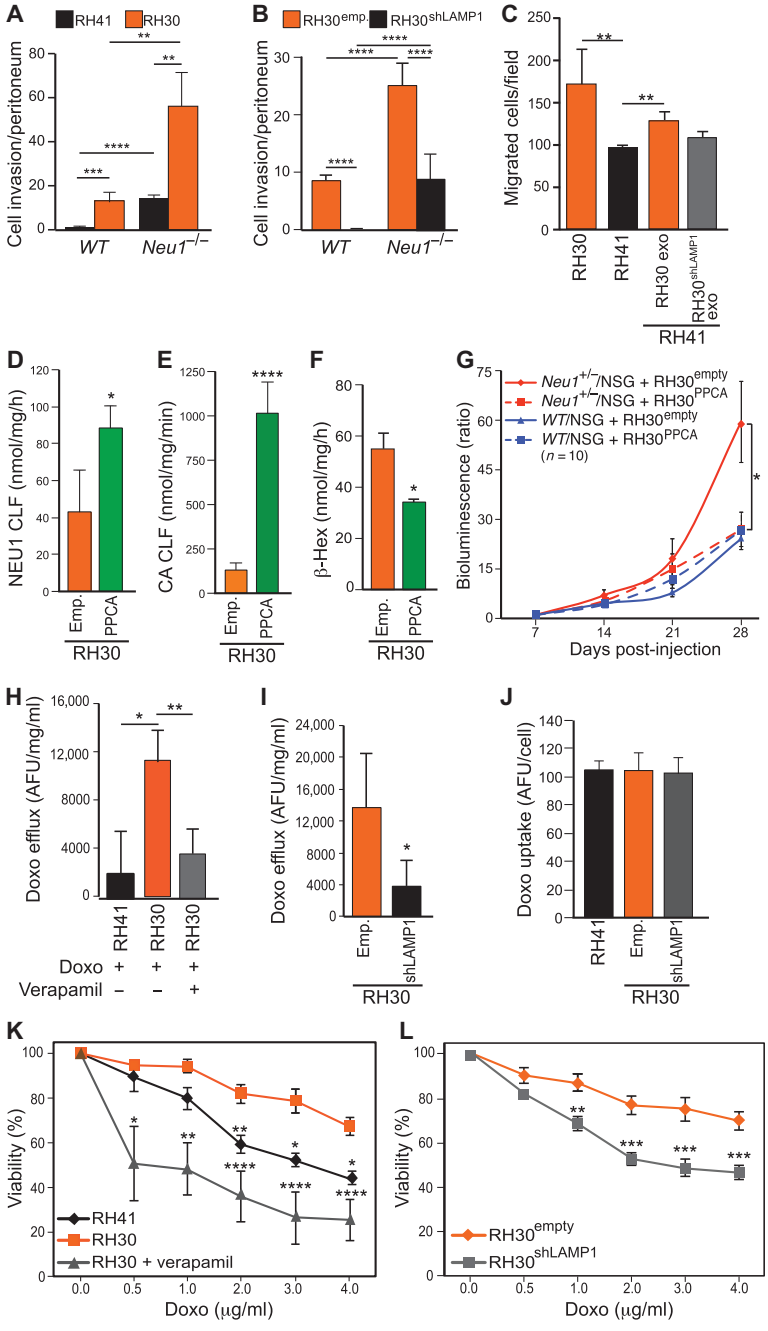

Fig. 6. NEU1 levels and the extent of lysosomal exocytosis in RMS cells determine their invasive potential and predict their responsiveness to chemotherapy. (**A**) Number of RH41 and RH30 cells that invaded ex vivo peritonea isolated from *Neu1*$^{+/+}$ (*WT*) or *Neu1*$^{-/-}$ mice (n = 10). (**B**) Number of RH30^{shLAMP1} cells and empty vector controls that invaded peritoneal membranes from *WT* or *Neu1*$^{-/-}$ mice (n = 5). (**C**) Number of RH30 and RH41 cells that migrated through a Matrigel Transwell chamber; number of migratory RH41 cells that were cultured in the presence of exosomes purified from RH30 or RH30^{shLAMP1} medium (exo) (n = 4). (**D**) NEU1 activity measured in a crude lysosomal fraction (CLF) of RH30^{PPCA} cells compared to that in the CLF of RH30^{empty} cells (n = 3). (**E**) Cathepsin A (CA) activity measured in CLF of RH30^{PPCA} cells compared to that in the CLF of RH30^{empty} cells (n = 10). (**F**) β-Hex activity assayed in the medium of RH30^{PPCA} cells was compared to that in the medium of RH30^{empty} control cells (n = 2). (**G**) Bioluminescence measurement of tumor growth after injection of RH30^{PPCA} and RH30^{empty} cells into the flank of *WT*/NSG (blue) or *Neu1*$^{+/-}$/NSG (red) mice. (**H**) Arbitrary fluorescence units (AFU) of doxorubicin (Doxo) effluxed into the medium by RH41 and RH30 cells after exposure to doxorubicin (4 μg/ml) alone or combined with 50 μM verapamil (n = 4). (**I**) AFU of doxorubicin effluxed into the medium of RH30^{shLAMP1} and RH30^{empty} cells after exposure to doxorubicin (4 μg/ml) (n = 4). (**J**) Quantification of the fluorescence intensity in individual RH41, RH30^{shLAMP1}, and RH30^{empty} cells after uptake of doxorubicin (n = 10). (**K**) Viability curves of RH41 and RH30 cells exposed for 16 hours to the indicated doses of doxorubicin alone or combined with 50 μM verapamil (n = 6). (**L**) Viability curves of RH30^{shLAMP1} and RH30^{empty} cells exposed for 16 hours to the indicated doses of doxorubicin (n = 6). Data are means ± SD or SEM. *P < 0.05, **P < 0.01, ***P < 0.005, ****P < 0.001, Student's t test for unpaired samples.

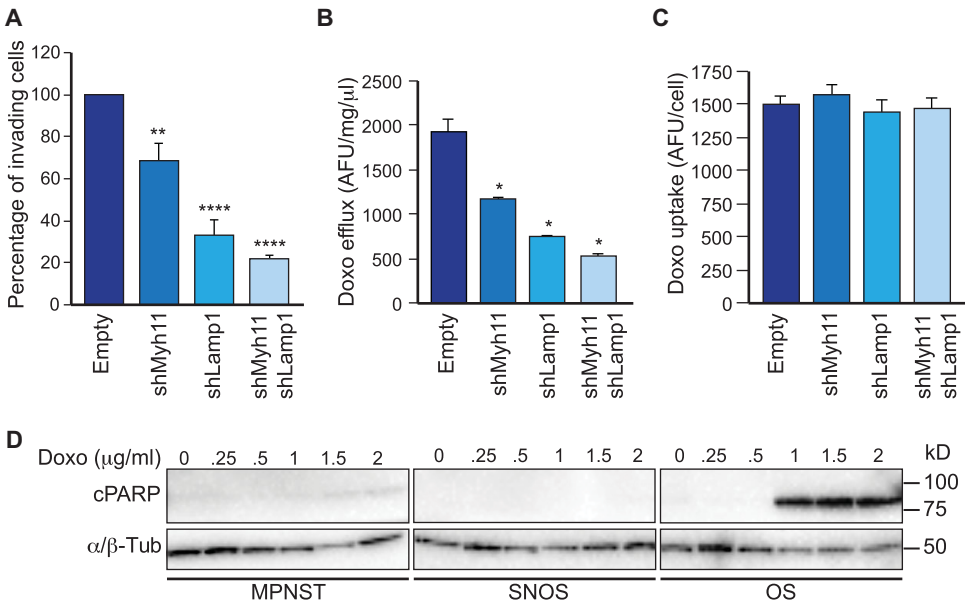

Fig. 7. The extent of lysosomal exocytosis in tumor cell lines derived from a *Neu1*$^{+/-}$/*Arf*$^{-/-}$ sarcoma determines their invasive potential and predicts their responsiveness to chemotherapy. (**A**) Number of sarcomas cells with silenced *Myh11* (shMyh11) and *Lamp1* (shLamp1) and with silencing of both *Lamp1* and *Myh11* (shLamp1/shMyh11) that migrated through a Matrigel Transwell chamber, compared with their empty vector control (n = 8). (**B**) Quantification of doxorubicin fluorescence (AFU) effluxed into the medium-modified sarcomas cells (shMyh11, shLamp1, and shLamp1/shMyh11) compared to their unmodified cells after exposure to doxorubicin (4 μg/ml) (n = 4). (**C**) Quantification of the fluorescence intensity in individual modified sarcoma cells (shMyh11, shLamp1, and shLamp1/shMyh11) compared to their unmodified cells after uptake of doxorubicin (n = 14). (**D**) Sensitivity to doxorubicin was assayed by cleaved poly(adenosine diphosphate–ribose) polymerase (cPARP) expression after exposing *Neu1*$^{+/-}$/*Arf*$^{-/-}$ sarcoma cells to the indicated doses of doxorubicin. α/β-Tubulin was used as the loading control. Data are means ± SD or SEM. *P < 0.05, **P < 0.01, ***P < 0.005, ****P < 0.001, Student's t test for unpaired samples.

enhanced lysosomal exocytosis (Fig. 5I). The invasive capacity of these cells was drastically reduced by silencing *Myh11*, *Lamp1*, or the combination of the two, suggesting again a link between lysosomal exocytosis and invasiveness in these cells (Fig. 7A). Intriguingly, the combined silencing of *Myh11* and *Lamp1* had a more robust effect than silencing the individual genes, suggesting a synergistic mode of action between the two proteins (Fig. 7A). We next measured the levels of doxorubicin effluxed by the silenced sarcoma cells and compared it to the levels measured in unmodified cells (Fig. 7B). Although all cells had a similar internalization of the drug (Fig. 7C), we measured a decreased efflux of doxorubicin in cells silenced for *Myh11*, *Lamp1*, or the combination of the two (Fig. 7B). These results suggest that in these primary sarcoma cells, Myosin-11 and Lamp1 cooperate in the process of lysosomal exocytosis to render the cells more invasive and drug-resistant.

Last, we demonstrated that our primary mouse sarcoma cell lines isolated from MPNST, SNOS, and OS with enhanced lysosomal exocytosis (Fig. 1H) were completely or partially resistant to doxorubicin exposure, as observed by the absence or low expression of the canonical apoptotic marker cPARP (Fig. 7D). Thus, excessive lysosomal exocytosis downstream of decreased NEU1 levels may be a mechanism that enables sarcomas to acquire resistance to lysosomotropic chemotherapeutics in vivo.

DISCUSSION

The genetic or epigenetic changes that cancer cells undergo during primary tumorigenesis may predispose them to respond to extrinsic cues that initiate an EMT process, allowing them to acquire a more aggressive phenotype (*40*). Among these changes is gaining the ability to alter cellular metabolic/catabolic machinery to create the most permissive conditions for invasion, dissemination, and survival (*41*). Many determinants of migration/invasion are cytoskeletal and vesicular trafficking components and biosynthetic/processing enzymes (*42*–*44*).

Here, we identified NEU1 as one such determinant. Altered sialic acid content on any NEU1 target affects its basic cellular pathways that are relevant for cancer progression, ranging from cell proliferation/differentiation and cell adhesion to receptor recognition, signal transduction, immune functions, and vesicular trafficking (*4*, *19*, *45*). We found that impaired sialic acid processing on LAMP1 directly affected lysosomal exocytosis, which we have now linked to the acquisition of an invasive, drug-resistant phenotype (*1*). The involvement of regulated lysosomal exocytosis in membrane dynamics, selective secretion of lysosomal contents, and remodeling of the PM and ECM (*1*, *46*, *47*) makes this process an ideal system for driving tumors into an aggressive state.

That lysosomal exocytosis indicates the development of the invasive phenotype of cancer cells in vivo is well exemplified in the *Neu1*$^{+/-}$/*Arf*$^{-/-}$ mouse model. In this genetic background, *Neu1* haploinsufficiency was sufficient to promote a high prevalence of pleomorphic sarcomas that resemble high-grade, pleomorphic soft tissue sarcomas in humans (*11*). Their morphologic similarities are reinforced by their common patterns of expression of markers that denote an ongoing EMT program. Execution of this program relies on intracellular signaling pathways orchestrated by specific protein kinases,

transcription factors and Rho guanosine triphosphatases (GTPases), as well as cell adhesion proteins (for example, β_4 integrin) (*40*). A possible mechanism implicating NEU1 down-regulation in the initiation of an EMT program is the occurrence of oversialylation of adhesion molecules such as β_4 integrin at the cell surface and LAMP1 at the lysosomal membrane. These combined sialic acid modifications on these NEU1 substrates would affect cell-cell communication and simultaneously exacerbate lysosomal exocytosis of soluble hydrolases and exosomes. This scenario would reconcile the early observations made in colon carcinoma cells, that is, that oversialylation of β_4 integrin activates the ERK1/2 signaling pathway, thereby increasing the cells' metastatic potential (*21*), with our current findings in sarcoma cells in which oversialylated LAMP1 enhances lysosomal exocytosis, making cancer cells migratory and invasive. We propose that enhanced lysosomal exocytosis of hydrolytic enzymes, combined with increased release of exosomes, cooperate in propagating signaling molecules to distant sites and educate an increasing number of cells to acquire EMT features. This hypothesis is in line with recent reports that implicate exosome-mediated delivery in the crosstalk between tumor and stroma in cancer progression (*27*–*31*).

Intracellular movement of lysosomes depends on their actin-mediated transport via members of the motor myosin family (*48*). Altered expression of motor myosins has been linked to cancer cell survival, invasion, and metastasis, indicating that cytoskeletal components mediating cell contractility and organelle trafficking function in cancer cell behavior (*44*, *49*). Recent examples are Myosin-X up-regulation in mutant p53–driven breast cancer models and Myosin-Va in colorectal cancer (*42*, *50*). In addition, up-regulation of other proteins involved in regulated exocytosis (that is, BAIAP3 and Rab27b) has been linked to tumorigenesis in desmoplastic small round cell tumor and breast cancer (*51*, *52*). We found that Myosin-11 and NEU1 are inversely expressed in metastatic and pleomorphic human LMS, in pleomorphic and recurrent RMS, and in the pleomorphic sarcomas with rhabdoid cells in our mouse model. This correlation extends the role of Myosin-11 in cancer progression. In addition, we demonstrated for the first time a direct interaction between Myosin-11 and LAMP1, specifically in aggressive sarcomas. This result supports the notion of strict cooperation between these two proteins in lysosomal trafficking and exocytosis, which ultimately determines the fate of cancer cells. Last, rhabdoid cells in the $Neu1^{+/-}/Arf^{-/-}$ pleomorphic sarcomas were Myosin-11^{+}, reiterating their similarity with their human counterparts and suggesting a common smooth muscle origin.

Studies of chemotherapy resistance have largely focused on the up-regulation of Pgp or other ABC transporters (*16*). However, specific inhibitors of these pumps have often proven unsuccessful in clinical trials (*53*), which suggests the existence of alternative efflux mechanisms. Sequestration of lysosomotropic drugs into acidic vesicles/lysosomes has been proposed as a means of multidrug resistance in multiple carcinoma cell lines (*16*, *53*, *54*), though the molecular mechanism(s) leading to the resistance phenotype has not been defined. We have now established that in chemoresistant, Pgp-negative RMS cells, lysosomotropic drugs are preferentially sequestered in lysosomes before being purged via NEU1-dependent enhanced lysosomal exocytosis.

In addition to low NEU1 expression being a potential risk factor in the development of aggressive cancer, we predict that other cues of neoplastic transformation place selective pressure on tumor cells to down-regulate *NEU1*, especially when they transition to an invasive/migratory disease. Whether low NEU1 expression is due to a preexisting deficiency or a transformation-related epigenetic change is currently unknown and will be further investigated. Supporting this prediction are two reports describing neoplastic malignancies that developed in three siblings with type I sialidosis with low NEU1 activity (*55*, *56*).

In conclusion, the dual action of NEU1 on processing sialoglycoconjugates and intracellular trafficking of lysosomes places it upstream of these events and suggests that this enzyme mediates specific stages of cancer progression. We propose that NEU1 expression coupled with lysosomal exocytosis effectors such as LAMP1 could be developed as diagnostic biomarkers and have potential as therapeutic targets for aggressive, untreatable human pleomorphic sarcomas.

MATERIALS AND METHODS

Experimental design

The main goal of this study was to understand the role of NEU1-dependent lysosomal exocytosis in tumor invasion and chemoresistance. We began with crossing $Neu1^{+/-}$ FVB/NJ mice with C57Bl6/129sv $Arf^{-/-}$ mice to assess the effect of *Neu1* haploinsufficiency on tumor burden and progression. Mice were monitored for tumor growth and euthanized following Institutional Animal Care and Use Committee and National Institutes of Health (NIH) guidelines. The St. Jude Veterinary Pathology Core (VPC) conducted extensive histological and immunohistochemical analyses of the tumors to diagnose and classify the different tumor types. We established primary tumor cell cultures from sarcomas resected from $Neu1^{+/-}/Arf^{-/-}$ mice to verify the occurrence of Neu1-dependent lysosomal exocytosis and chemoresistance. This was done using enzyme activity assays to determine Neu1 activity, β-Hex activity in the culture medium, and Western blotting to detect Lamp1. These results prompted us to test human sarcoma TMAs (LMS and RMS) for expression levels of NEU1 and LAMP1, the key regulators of lysosomal exocytosis. Our certified pathologist scored the expression levels of the two proteins.

We used two RMS cell lines expressing distinct levels of NEU1 to dissect the lysosomal exocytosis pathway in vitro. RT-qPCR, Western blotting, and enzyme activity assays were used to determine NEU1 expression and activity as well as LAMP1 expression. The latter was shown to be oversialylated in the low-NEU1 RMS cells compared to the high-NEU1 RMS cells by using sialic acid binding specific lectins (SNA and MAL). RMS cells were genetically engineered using a lentiviral infection system to prove that by varying NEU1 expression or knocking down LAMP1, we could directly influence the extent of lysosomal exocytosis. Exocytosed exosomes were also found to be greater in low-NEU1 RMS cells. Finally, live TIRF microscopy showed that the number of lysosomes docked at the cell surface and ready to exocytose was inversely proportional to the levels of NEU1.

A large gene data set (GSE21050) comprising 309 human sarcomas was queried by our computational biologist for *NEU1* correlative gene expression. The results obtained herein were then verified in the LMS and RMS included in the human TMAs, in patient-derived xenografts of RMS, in tumors from our $Neu1^{+/-}/Arf^{-/-}$ mouse model, and in the cells derived from these sarcomas. To determine whether Lamp1 and Myosin-11 interact, we coimmunoprecipitated the two proteins in a sarcoma cell line from a $Neu1^{+/-}/Arf^{-/-}$ mouse, and Myosin-11 function in lysosomal exocytosis was further verified by silencing *Myo11* and assaying lysosomal exocytosis effect by enzyme activity.

To show that NEU1-dependent exacerbation of lysosomal exocytosis increased the invasive capacity of tumors, we performed ex vivo invasion assays by seeding RMS cells onto peritonea from *Neu1*$^{+/+}$ or *Neu1*$^{-/-}$ mice and counting the number of cells that invaded the basement membrane. Transwell chamber migration assays were also used to show that exosomes from low-NEU1 and high-LAMP1 cells induced migration of high-NEU1, low-LAMP1 cells. These results were validated in vivo using orthotopic xenografts of low-NEU1– and high-NEU1–expressing RMS cells (transfected with a luciferase construct) injected into the flank muscle of *Neu1*$^{+/+}$/NSG or *Neu1*$^{+/-}$/NSG mice. Tumor growth was monitored by quantification of luciferase by bioluminescence imaging. Finally, to verify that exacerbated lysosomal exocytosis in RMS cells with low-NEU1 expression conferred chemoresistance by the efflux of lysosome-sequestered drugs, we exposed cells to doxorubicin and quantified the release of its native fluorescence into the culture medium. Viability curves of RMS cells exposed to increasing concentrations of doxorubicin were also done to assess the extent of the cells' resistance. Drug resistance could be reverted by using the calcium channel blocker verapamil. Additionally, we used the apoptotic marker cPARP to show that primary cells derived from *Neu1*$^{+/-}$/*Arf*$^{-/-}$ mice with increased lysosomal exocytosis were resistant to doxorubicin exposure.

Animals

All procedures were performed per NIH guidelines and animal protocols approved by our Institutional Animal Care and Use Committee. *Neu1*$^{+/-}$ FVB/NJ mice were crossed with NSG or C57Bl6/129sv *Arf*$^{-/-}$ mice (provided by C. Sherr). For orthotopic xenografts, 2×10^6 RMS cells were engrafted into the flanks of 4- to 6-week-old *Neu1*$^{+/+}$/NSG or *Neu1*$^{+/-}$/NSG male mice. Mice were intraperitoneally injected with Firefly D-Luciferin (3 mg/mouse, Caliper Life Sciences) and imaged with the IVISH 200 system. Living Image 3.2 software (Caliper Life Sciences) was used to generate a standard region of interest (ROI), encompassing the largest tumor at maximal bioluminescence signal. The same ROI was used to determine the mean radiance (photons/s per cm^2 per sr) for xenografts at all time points. Human RMS xenografts were generated as previously described (*24*). Samples of primary human RMS were obtained under Institutional Review Board approval, in accordance with NIH policies and guidance for human subjects, and implanted subcutaneously onto the flanks of male CB17 *scid*$^{-/-}$ mice (6 to 8 weeks old, Taconic Farms). Once the initial transplant grew to sufficient size, the tumors were serially propagated by subsequent transplantation into healthy mice. The VPC staff performed full necropsies.

Cell culture

RH41 and RH30 cell lines were provided by G. Grosveld and C. L. Morton. Establishment of primary cells from *Arf*$^{-/-}$/*Neu1*$^{+/-}$ mice was done following G. Grosveld's procedure: tumors were dissected, minced, and digested at 37°C for 45 min in Hanks' balanced salt solution supplemented with Liberase TL (Roche). The cell suspensions were filtered through 70-μm cell strainers, and cells were maintained in standard growth conditions. All cells were maintained in Dulbecco's modified Eagle's medium (DMEM) or RPMI (Cellgro) and supplemented with 10% cosmic calf serum (CCS), 2 mM Glutamax, penicillin (100 U/ml), and streptomycin (100 μg/ml) (Life Technologies).

RH41 cells were transfected with five short hairpin RNA (shRNA) constructs for human *NEU1* gene cloned into the pLKO1 HIV-based lentiviral vector (TRC-Hs1.0 RHS4533-NM000434, Open Biosystems). RH30 cells were transfected with the pBABE-puro plasmid (AddGene) containing the human *NEU1* complementary DNA by using the Fugene6 Transfection Reagent protocol (Roche). For lentiviral transduction, vectors were produced by cotransfection of 293T cells with 10 μg of pCAGkGP1R and 2 μg of pCAG4RTR2 packaging plasmids, 2 μg of pCAG-VSVG envelope plasmid, and 10 μg of vector plasmid, as previously described (*57*). The packaging and envelope plasmids were gifts from D. Persons. RH30 cells were transduced with five shRNA constructs for human *LAMP1* gene cloned into the pLKO1 HIV-based lentiviral vector plasmid (TRC-Hs1.0 RHS3979-9596672, Open Biosystems), or RH30 cells were transduced with lentiviral vector containing the human *PPCA* gene (pCL20c-PPCA-GFP) followed by transduction with a pCL20c-Luciferase2-IRES-YFP plasmid. The primary sarcoma cell line was transduced with five shRNA constructs for mouse *Myh11* and mouse *Lamp1* genes cloned into the pLKO1 HIV-based lentiviral vector plasmid (TRC-Mn1.0 RMM4534-EG17880, RMM4534-EG16783 Dharmacon RNAi, GE Healthcare). Empty vectors were used as controls. Stable cells were selected with puromycin (2 μg/ml) or fluorescence-activated cell sorting (FACS)–sorted for green fluorescent protein (GFP) and yellow fluorescent protein (YFP) and screened for luciferase activity.

Gene expression by RT-qPCR

RNA was isolated with TRIzol (Invitrogen), and reverse transcription PCR was performed using the SuperScript III First-Strand (Invitrogen). RT^2 SYBR Green/Fluorescein qPCR Mastermix (SABiosciences) was used for real-time qPCR, which was performed using a Bio-Rad iQ5 iCycler with the Optical System Software 1.0, using RT^2 SYBR Green/Fluorescein qPCR Mastermix (SABiosciences) following the manufacturer's protocol. Primers used were human *NEU1* (PPH11418A, SABiosciences). Data were normalized to endogenous hypoxanthine phosphoribosyltransferase 1 (HPRT1) (PPH01018, SABiosciences).

Immunohistochemistry

Tissues were dewaxed, and antigen retrieval was performed using citrate buffer (0.1 M citric acid and 0.1 M sodium citrate, pH 6.0). Slides were blocked [0.1% bovine serum albumin (BSA) and 0.5% Tween 20 with 10% normal goat serum] and incubated with the following primary antibodies overnight: anti-NEU1 (1:50) (*58*), anti-LAMP1 (1:400) (Cell Signaling), and anti–Myosin-11 (1:300) (Millipore and LSBio). Slides were incubated for 1 hour with biotinylated secondary antibodies (Jackson ImmunoResearch Laboratory). Endogenous peroxidase was removed with 0.1% hydrogen peroxidase for 30 min. Antibody detection was performed using the ABC Kit and DAB substrate (Vector Laboratories). Slides were counterstained with H&E. Human cancer TMAs were obtained from US Biomax Inc. and blindly graded by a pathologist in the VPC. Immunohistochemical analysis was done using Target Retrieval Solution, pH 9 (DAKO), for 30 min at 98°C. Primary antibodies used were anti-cytokeratin OSCAR (1:100) and anti-vimentin (1:20). Both were blocked with Background Sniper for 30 min (BioCare Medical), incubated with streptavidin horseradish peroxidase (HRP) (Thermo Fisher) for 10 min and DAB (DAKO) for 10 min, and then counterstained with H&E. Immunohistochemical analysis of TGFβ was done using the antibody at 1:100 dilution followed by methyl green counterstaining. The following primary antibodies were used: anti-cytokeratin OSCAR (SIG-3465, Covance), anti-vimentin (EPR3776, Novus Biologicals), anti-laminin (L9393 Sigma), anti–collagen IV (#2150/1470, AbD Serotec),

and anti-TGFβ (T 0438, Sigma). The level of NEU1 and LAMP1 was subjectively graded on the basis of comparison to labeling of vascular smooth muscle cells within the tumors. Labeling of tumor cells with similar intensity to these cells was considered moderate, and labeling that was stronger or weaker was considered high or low, respectively.

Confocal analysis

For NEU1 immunofluorescence, cells were fixed for 10 min in chilled 95% ethanol and 5% acetic acid, followed by 1-hour blocking with Image-iT signal enhancer (Molecular Probes) and incubation with primary antibody (1:50) in 25 mM Na-phosphate, 150 mM NaCl, 1% BSA, and 0.3% gelatin overnight at 4°C. For LAMP1 immunofluorescence, cells were fixed with either 3.7% formaldehyde (nonpermeabilized) or 4% paraformaldehyde (permeabilized). Slides were blocked with Image-iT for 20 min. Cells were incubated with anti-LAMP1 antibody (1:200) overnight at 4°C in 100 mM Na-phosphate and 100 mM NaCl (pH 7.2). After 1-hour incubation with secondary Alexa Fluor (1:400, Invitrogen), slides were mounted with ProLong Gold antifade reagent with 4′,6-diamidino-2-phenylindole (DAPI) (Invitrogen). For LysoTracker fluorescence microscopy, cells were incubated for 30 min at 37°C in medium containing 200 nM LysoTracker as reported previously (*1*). Confocal analysis on LysoTracker-stained live cells was performed with an inverted microscope equipped with a C1Si confocal system. Lysosomes were identified as objects and counted in more than 10 images. To determine the perinuclear region, we drew a closed boundary of 3 to 5 μm outside the nuclear envelope and assessed the number of lysosomes in this region. The "peripheral" ROI was considered as the rest of the cytoplasm.

TIRF microscopy

Live TIRF microscopy (*59*) was performed with either a Zeiss Elyra PS1 or a Marianas imaging system (Intelligent Imaging Innovations) consisting of a Zeiss Axio Observer motorized inverted microscope with a TIRF illuminator (Carl Zeiss MicroImaging). Images were acquired with an Alpha Plan-Apochromat 100× 1.46 oil objective. Monochrome images were analyzed with NIS-Elements 4.13.

Lysosomal tethering/docking quantification

The evanescent wave field depth was 100 nm. Live TIRF image analysis was performed with the Elements software (Nikon). Thresholds for intensity and size were set at the beginning of the analysis and kept for the duration of all the analyses. For two-dimensional tracking, we selected the lysosomes with "AutoDetect All" of "Define New ROI" in the "Tracking" module (under "Analysis Controls"). Any lysosome with a total path length less than or equal to 1 μm during a period of 10 s was defined as tethered/docked.

Immunoblotting

Western blots were performed as previously described (*7*). Briefly, cells were lysed in radioimmunoprecipitation assay buffer [50 mM tris-HCl (pH 7.5), 150 mM NaCl, 0.1% SDS, 1% sodium deoxycholate, 1% Triton X-100, 1:50 Complete protease inhibitor cocktail (Roche)], and lysates were separated by SDS–polyacrylamide gel electrophoresis gels. Nitrocellulose or polyvinylidene difluoride (PVDF) membranes were blocked for 1 hour with 5% nonfat milk and subsequently probed with primary antibodies overnight: anti-LAMP1 (1:2000, Cell Signaling or BD Biosciences), anti-MYH11 (1:1000, LSBio or Proteintech), anti-cPARP, anti–α/β-tubulin (1:1000, Cell Signaling), and anti-NEU1 (1:250) (*58*). After washing, blots were incubated for 1 hour with HRP-conjugated secondary antibodies. Immunoblots were developed using SuperSignal West Pico Chemiluminescent Substrate (Thermo Scientific). Anti-Pgp was a gift from E. Schuetz. Lysosomes were purified from RH30 Empty and RH30 PPCA using the Lysosome Isolation Kit (Sigma) following the manufacturer's protocol with slight modifications. In brief, cells were lysed in four volumes of 1× extraction buffer in a glass Dounce homogenizer. The nuclei were removed by centrifugation at 1000*g* for 10 min. The postnuclear supernatant was then centrifuged at 20,000*g* for 20 min, and the resulting pellet, containing the CLF, was resuspended in a minimal volume of 1× extraction buffer and subjected to enzymatic assays and Western blot analysis.

Enzyme activity

NEU1 and β-Hex enzymatic activities were measured with the appropriate fluorimetric substrates (Sigma), as described previously (*1*), and their activity was normalized for protein concentrations. Medium collected at 16 hours of culture was spun through a Sephadex column at pH 5.5 for 1 min at 850*g* to normalize the pH of all samples before analysis.

Immunoprecipitation

For Lamp1 immunoprecipitation, primary sarcoma cells were lysed in CHAPS buffer [50 mM Pipes/HCl (pH 6.5), 2 mM EDTA, 0.1% CHAPS, leupeptin (20 μg/ml), pepstatin A (10 μg/ml), and aprotinin (10 μg/ml)]. Total proteins (250 μg) were incubated overnight at 4°C on a rotating platform with 2 μg of anti-LAMP1 antibody (BD Biosciences) or normal immunoglobulin G (IgG) (Santa Cruz Biotechnology). Dynabeads Protein G (Novex, Life Technologies) were simultaneously incubated with V5 tag (1 μg/ml) antibody–blocking peptide. Beads were washed and added to the cell lysates; samples were incubated for an additional hour. The beads were then washed four times in CHAPS buffer, and proteins were eluted with sample loading buffer before immunoblotting. For Myosin-11 immunoprecipitation, primary sarcoma cells were subjected to subcellular fractionation using a procedure adapted from Yang and Robbins (*28*) to enrich for the membrane fraction containing the cytoskeletal compartment. In brief, cells were lysed in ice-cold buffer A [containing 320 nM sucrose, 10 mM tris base, 5 mM NaF, 1 mM Na_3VO_4, 1 mM EDTA, 1 mM EGTA (pH 7.4), 1:50 Complete protease inhibitor cocktail (Roche)] using a Dounce homogenizer. Homogenates were centrifuged for 10 min at 800*g* at 4°C. The supernatant S1 was then centrifuged for 2 hours at 165,000*g* at 4°C. The pellet P2 was then solubilized in ice-cold buffer B (containing 1% sodium deoxycholate, 10 mM tris base, 5 mM NaF, 1 mM Na_3VO_4, 1 mM EDTA, 1 mM EGTA, protease inhibitors) and subjected to immunoprecipitation experiments using 2 μg of anti-MYH11 antibody (Abcam) or nonspecific IgG. After being transferred to a PVDF membrane, immunoprecipitated proteins were probed with anti-MYH11 (1:1000, Proteintech) or anti-LAMP1 (1:500, BD Biosciences) antibodies. Immunoblot was probed with anti-CD63 (1:250, Santa Cruz Biotechnology) to test specificity of interaction between Myo11 and Lamp1.

Dextran exocytosis and uptake

Cells (6×10^4) were incubated for 2 hours with Alexa Fluor 594–conjugated dextran (0.5 mg/ml; molecular weight, 10,000; anionic) (Life Technologies) to allow for complete endocytosis followed by redistribution and accumulation of the compound in the lysosomes (*58*). Cells were washed four times with phosphate-buffered saline (PBS),

and the medium was changed. After 1 hour, the medium was spun down and exocytosed. Alexa Fluor 594–dextran fluorescence was measured (excitation, 585/10 nm; emission, 615/10 nm). AFU were normalized to protein concentration.

For dextran uptake, cells were incubated with Alexa Fluor 594–conjugated dextran (0.5 mg/ml; molecular weight, 10,000). After 30 min, cells were washed twice with PBS and imaged with a Nikon C1 confocal system mounted on a Nikon TE2000 inverted microscope fitted with an incubator chamber for humidity, CO_2, and temperature control. Seven to 10 images were acquired for each group of cells. The fluorescence intensity (in arbitrary units) of the red channel was determined for individual cells; the mean + SD are shown in the graph.

Doxorubicin efflux, uptake, and cytotoxicity

Cells (6×10^4) were treated with doxorubicin [4 μg/ml (0.04 μM) or 6 μg/ml (0.06 μM)] (LKT Laboratories) for 2 hours. Cells were washed four times with PBS, and the medium was changed. After 2 hours, the medium was spun down, and the native red fluorescence of exocytosed doxorubicin was measured (excitation, 485/12 nm; emission, 590/10 nm). AFU were normalized to protein concentration.

For doxorubicin uptake, cells (1.5×10^5) were plated. The next day, cells were treated with doxorubicin (t_0). After 30 min of incubation with the drug (t_{30}), cells were imaged. Quantification of the fluorescence intensity of the red channel (emission) was assessed as a measure of the amount of doxorubicin uptake.

For cytotoxicity assays, cells were treated with doxorubicin (0.5 to 4 μg/ml) for 16 hours with or without 50 μM verapamil (Sigma). For quantification of viability, the CellTiter 96 AQ_{ueous} One Solution Reagent (Promega) was added to the culture medium, following the manufacturer's instructions. Absorbance at 490 nm was recorded by measuring the quantity of formazan, which is directly proportional to the absorbance at 490 nm.

Exosome isolation and characterization

Cells were cultured in DMEM containing 10% CCS depleted from contaminating vesicles by ultracentrifugation for 16 hours at 100,000*g*. Cultured medium was collected after 16 hours, and crude exosomes were purified by several centrifugation steps: 10 min at 300*g*; 10 min at 1200*g*; 30 min at 10,000*g*; 2 hours at 100,000*g*, all at 4°C. The pellet was washed with cold PBS and centrifuged for 2 hours at 100,000*g*. Quantification of total protein from the resulting pellet was done using the bicinchoninic acid (BCA) method. Western blots of exosomal preparations were probed overnight with antibodies against characterized exosomal proteins (*32*, *60*): anti-CD81 (Santa Cruz Biotechnology, 1:250), anti–flotillin-1 (BD Biosciences, 1:500), anti–syndecan-1 (Life Technologies, 1:250), and anti–syntenin-1 (Millipore, 1:1000).

Ex vivo invasion assay

Neu1$^{+/+}$ or *Neu1*$^{-/-}$ peritonea were mounted over Transwell inserts (Fisher) and processed as previously described (*61*). RMS cells (2.5×10^5) were overlaid onto the peritoneum and maintained in culture for 8 days. Peritonea were fixed, embedded in paraffin, cross-sectioned, and stained with H&E. The numbers of invading cells throughout the length of different peritonea were counted.

Transwell migration assay and exosome uptake

RMS and primary sarcoma cell line invasion/migration was done following the manufacturer's instructions (Corning Biocoat Matrigel Invasion Chambers, Corning). Migrated cells were counted from several replicates from two independent experiments. For exosome uptake, cells were incubated with exosomes (10 μg/ml) for 16 hours, and the number of migrated cells was quantified.

Sialoglycoprotein purification with lectins

SNA and MAL lectin spin columns were used for specific enrichment of glycoproteins with sialic acid–rich glycan moieties from RH41 and RH30 cells, following the manufacturer's protocol (Qproteome Sialic Glycoprotein Kit, Qiagen). The same numbers of cells were used to load the columns. The SNA column binds to Neu5Acα2-6Gal(NAc)-R, and the MAL column binds to Neu5Ac/Gcα2-3Galβ1-4GlcNAcβ1-R. The resulting sialic acid–enriched glycoproteins were immunoblotted and probed with anti-LAMP1 (1:2000; Cell Signaling) antibody.

Gene expression analysis of human sarcomas

Microarray data from Affymetrix HG-U133 plus 2 arrays were used (GSE21050), robust multiarray average (RMA)–normalized, and summarized using Partek Genomics Suite version 6.6. Principal components analysis and quality control metrics identified two outlier samples (removed), leaving 308 sarcoma samples. Pearson and Spearman correlations were used to correlate the NEU1 probe set with all other probe sets, and a false discovery rate (q value) was calculated.

Statistical analysis

Data values were expressed as means ± SD or SEM of at least two independent experiments and evaluated using Student's t test for unpaired samples. Activity assays from primary sarcoma cells were compared using one-way analysis of variance (ANOVA) unpaired t test. For scatterplots, linear fits, and box plots, unequal variance t tests and one-way ANOVA of $\log_2$ expression were calculated using STATA/MP 11.2. Mean differences were considered significant when $P < 0.05$.

SUPPLEMENTARY MATERIALS

Supplementary material for this article is available at http://advances.sciencemag.org/cgi/content/full/1/11/e1500603/DC1

Fig. S1. UPS that developed in a *Neu1*$^{+/-}$/*Arf*$^{-/-}$ mouse expresses epithelial and mesenchymal markers and TGFβ.

Fig. S2. Excessive lysosomal exocytosis in RMS cells is caused by low NEU1 and high LAMP1 levels.

Fig. S3. Genes whose expression is negatively correlated with that of *NEU1* expression in a sarcoma data set (GSE21050).

Fig. S4. Showing of entire immunoblots corresponding to panels in Fig. 5 (E and F).

Fig. S5. Immunoprecipitation of Myosin-11 and CD63.

Fig. S6. NEU1 expression levels in tumor cells and the surrounding microenvironment determine their invasiveness.

Fig. S7. Increased lysosomal exocytosis confers chemoresistance to RMS cells.

Table S1. Type of tumors developed in *Neu1*$^{+/+}$/*Arf*$^{-/-}$ and *Neu1*$^{+/-}$/*Arf*$^{-/-}$ mice.

Table S2. Immunohistochemical markers used for diagnosis of sarcomas.

Table S3. Metastasis status in the sarcoma data set (GSE21050).

Movie S1. In RH41 cells, lysosomes localize in the perinuclear region.

Movie S2. In RH30 cells, lysosomes distribute to the cell periphery.

Movie S3. Live TIRF imaging of LysoTracker-labeled lysosomes in RH41 as a measure of tethering to or docked at the PM.

Movie S4. Live TIRF imaging of LysoTracker-labeled lysosomes in RH30 as a measure of tethering to or docked at the PM.

Movie S5. Doxorubicin exposure induces lysosome aggregation and subsequent apoptosis of RH41 cells.

Movie S6. RH30 cells maintain lysosomal trafficking and are resistant to doxorubicin exposure.

Movie S7. In RH41 cells, doxorubicin concentrates primarily in the nucleus.

Movie S8. In RH30 cells, a fraction of doxorubicin remains lysosomal.

Movie S9. RH30 cells cotreated with doxorubicin and verapamil cluster lysosomes in the perinuclear region and undergo apoptosis.

REFERENCES AND NOTES

1. G. Yogalingam, E. J. Bonten, D. van de Vlekkert, H. Hu, S. Moshiach, S. A. Connell, A. d'Azzo, Neuraminidase 1 is a negative regulator of lysosomal exocytosis. *Dev. Cell* **15**, 74–86 (2008).
2. A. Rodriguez, P. Webster, J. Ortego, N. W. Andrews, Lysosomes behave as Ca^{2+}-regulated exocytic vesicles in fibroblasts and epithelial cells. *J. Cell Biol.* **137**, 93–104 (1997).
3. P. E. Kima, B. Burleigh, N. W. Andrews, Surface-targeted lysosomal membrane glycoprotein-1 (Lamp-1) enhances lysosome exocytosis and cell invasion by *Trypanosoma cruzi*. *Cell. Microbiol.* **2**, 477–486 (2000).
4. E. Monti, E. Bonten, A. D'Azzo, R. Bresciani, B. Venerando, G. Borsani, R. Schauer, G. Tettamanti, Sialidases in vertebrates: A family of enzymes tailored for several cell functions. *Adv. Carbohydr. Chem. Biochem.* **64**, 403–479 (2010).
5. G. H. Thomas, in *The Metabolic and Molecular Bases of Inherited Disease,* C. R. Scriver, A. L. Beaudet, W. S. Sly, D. Valle, Eds. (McGraw Hill Inc., New York, 2001), vol. III, pp. 3507–3534.
6. A. d'Azzo, E. H. Kolodny, E. Bonten, I. Annunziata, in *Hematology of Infancy and Childhood*, S. H. Orkin, D. G. Nathan, D. Ginsburg, A.T. Look, D. E. Fisher, S. E. Lux, Eds. (Saunders Elsevier, Philadelphia, PA, 2009).
7. E. Zanoteli, D. van de Vlekkert, E. J. Bonten, H. Hu, L. Mann, E. M. Gomero, A. J. Harris, G. Ghersi, A. d'Azzo, Muscle degeneration in neuraminidase 1-deficient mice results from infiltration of the muscle fibers by expanded connective tissue. *Biochim. Biophys. Acta* **1802**, 659–672 (2010).
8. I. Annunziata, A. Patterson, D. Helton, H. Hu, S. Moshiach, E. Gomero, R. Nixon, A. d'Azzo, Lysosomal NEU1 deficiency affects amyloid precursor protein levels and amyloid-β secretion via deregulated lysosomal exocytosis. *Nat. Commun.* **4**, 2734 (2013).
9. J. Toguchida, T. Nakayama, Molecular genetics of sarcomas: Applications to diagnoses and therapy. *Cancer Sci.* **100**, 1573–1580 (2009).
10. L. Guillou, A. Aurias, Soft tissue sarcomas with complex genomic profiles. *Virchows Archiv.* **456**, 201–217 (2010).
11. Y. Oda, M. Tsuneyoshi, Extrarenal rhabdoid tumors of soft tissue: Clinicopathological and molecular genetic review and distinction from other soft-tissue sarcomas with rhabdoid features. *Pathol. Int.* **56**, 287–295 (2006).
12. Y. Oshiro, H. Shiratsuchi, Y. Oda, S. Toyoshima, M. Tsuneyoshi, Rhabdoid features in leiomyosarcoma of soft tissue: With special reference to aggressive behavior. *Mod. Pathol.* **13**, 1211–1218 (2000).
13. M. M. Nicolas, P. Tamboli, J. A. Gomez, B. A. Czerniak, Pleomorphic and dedifferentiated leiomyosarcoma: Clinicopathologic and immunohistochemical study of 41 cases. *Hum. Pathol.* **41**, 663–671 (2010).
14. A. J. Bathan, A. Constantinidou, S. M. Pollack, R. L. Jones, Diagnosis, prognosis, and management of leiomyosarcoma: Recognition of anatomic variants. *Curr. Opin. Oncol.* **25**, 384–389 (2013).
15. C. Forscher, M. Mita, R. Figlin, Targeted therapy for sarcomas. *Biologics* **8**, 91–105 (2014).
16. N. Raghunand, R. Martínez-Zaguilan, S. H. Wright, R. J. Gillies, pH and drug resistance. II. Turnover of acidic vesicles and resistance to weakly basic chemotherapeutic drugs. *Biochem. Pharmacol.* **57**, 1047–1058 (1999).
17. M. N. Christiansen, J. Chik, L. Lee, M. Anugraham, J. L. Abrahams, N. H. Packer, Cell surface protein glycosylation in cancer. *Proteomics* **14**, 525–546 (2014).
18. M. Hedlund, E. Ng, A. Varki, N. M. Varki, α2-6–Linked sialic acids on N-glycans modulate carcinoma differentiation in vivo. *Cancer Res.* **68**, 388–394 (2008).
19. T. Miyagi, K. Takahashi, K. Hata, K. Shiozaki, K. Yamaguchi, Sialidase significance for cancer progression. *Glycoconj. J.* **29**, 567–577 (2012).
20. T. Miyagi, T. Wada, K. Yamaguchi, K. Shiozaki, I. Sato, Y. Kakugawa, H. Yamanami, T. Fujiya, Human sialidase as a cancer marker. *Proteomics* **8**, 3303–3311 (2008).
21. T. Uemura, K. Shiozaki, K. Yamaguchi, S. Miyazaki, S. Satomi, K. Kato, H. Sakuraba, T. Miyagi, Contribution of sialidase NEU1 to suppression of metastasis of human colon cancer cells through desialylation of integrin β4. *Oncogene* **28**, 1218–1229 (2009).
22. T. Kamijo, S. Bodner, E. van de Kamp, D. H. Randle, C. J. Sherr, Tumor spectrum in *ARF*-deficient mice. *Cancer Res.* **59**, 2217–2222 (1999).
23. Y. Oda, K. Miyajima, K.-i. Kawaguchi, S. Tamiya, Y. Oshiro, Y. Hachitanda, M. Oya, Y. Iwamoto, M. Tsuneyoshi, Pleomorphic leiomyosarcoma: Clinicopathologic and immunohistochemical study with special emphasis on its distinction from ordinary leiomyosarcoma and malignant fibrous histiocytoma. *Am. J. Surg. Pathol.* **25**, 1030–1038 (2001).
24. C. L. Morton, R. A. Papa, R. B. Lock, P. J. Houghton, Preclinical chemotherapeutic tumor models of common childhood cancers: Solid tumors, acute lymphoblastic leukemia, and disseminated neuroblastoma. *Curr. Protoc. Pharmacol.* **Chapter 14**, Unit14.8 (2007).
25. P. J. Houghton, C. L. Morton, C. Tucker, D. Payne, E. Favours, C. Cole, R. Gorlick, E. A. Kolb, W. Zhang, R. Lock, H. Carol, M. Tajbakhsh, C. P. Reynolds, J. M. Maris, J. Courtright, S. T. Keir, H. S. Friedman, C. Stopford, J. Zeidner, J. Wu, T. Liu, C. A. Billups, J. Khan, S. Ansher, J. Zhang, M. A. Smith, The pediatric preclinical testing program: Description of models and early testing results. *Pediatr. Blood Cancer* **49**, 928–940 (2007).
26. X. Wu, K. A. Steigelman, E. Bonten, H. Hu, W. He, T. Ren, J. Zuo, A. d'Azzo, Vacuolization and alterations of lysosomal membrane proteins in cochlear marginal cells contribute to hearing loss in neuraminidase 1-deficient mice. *Biochim. Biophys. Acta* **1802**, 259–268 (2010).
27. H. Peinado, S. Lavotshkin, D. Lyden, The secreted factors responsible for pre-metastatic niche formation: Old sayings and new thoughts. *Semin. Cancer Biol.* **21**, 139–146 (2011).
28. C. Yang, P. D. Robbins, The roles of tumor-derived exosomes in cancer pathogenesis. *Clin. Dev. Immunol.* 2011, 842849 (**2011**).
29. A. Janowska-Wieczorek, M. Wysoczynski, J. Kijowski, L. Marquez-Curtis, B. Machalinski, J. Ratajczak, M. Z. Ratajczak, Microvesicles derived from activated platelets induce metastasis and angiogenesis in lung cancer. *Int. J. Cancer* **113**, 752–760 (2005).
30. V. Luga, L. Zhang, A. M. Viloria-Petit, A. A. Ogunjimi, M. R. Inanlou, E. Chiu, M. Buchanan, A. N. Hosein, M. Basik, J. L. Wrana, Exosomes mediate stromal mobilization of autocrine Wnt-PCP signaling in breast cancer cell migration. *Cell* **151**, 1542–1556 (2012).
31. P. Vader, X. O. Breakefield, M. J. A. Wood, Extracellular vesicles: Emerging targets for cancer therapy. *Trends Mol. Med.* **20**, 385–393 (2014).
32. S. Mathivanan, C. J. Fahner, G. E. Reid, R. J. Simpson, ExoCarta 2012: Database of exosomal proteins, RNA and lipids. *Nucleic Acids Res.* **40**, D1241–D1244 (2012).
33. F. Chibon, P. Lagarde, S. Salas, G. Pérot, V. Brouste, F. Tirode, C. Lucchesi, A. de Reynies, A. Kauffmann, B. Bui, P. Terrier, S. Bonvalot, A. Le Cesne, D. Vince-Ranchère, J.-Y. Blay, F. Collin, L. Guillou, A. Leroux, J.-M. Coindre, A. Aurias, Validated prediction of clinical outcome in sarcomas and multiple types of cancer on the basis of a gene expression signature related to genome complexity. *Nat. Med.* **16**, 781–787 (2010).
34. G. Fang, D. Zhang, H. Yin, L. Zheng, X. Bi, L. Yuan, Centlein mediates an interaction between C-Nap1 and Cep68 to maintain centrosome cohesion. *J. Cell Sci.* **127**, 1631–1639 (2014).
35. M.-H. Cuif, F. Possmayer, H. Zander, N. Bordes, F. Jollivet, A. Couedel-Courteille, I. Janoueix-Lerosey, G. Langsley, M. Bornens, B. Goud, Characterization of GAPCenA, a GTPase activating protein for Rab6, part of which associates with the centrosome. *EMBO J.* **18**, 1772–1782 (1999).
36. A. M. Belkin, I. V. Klimanskaya, M. E. Lukashev, K. Lilley, D. R. Critchley, V. E. Koteliansky, A novel phosphoglucomutase-related protein is concentrated in adherens junctions of muscle and nonmuscle cells. *J. Cell Sci.* **107** (Pt. 1), 159–173 (1994).
37. G. J. Babu, D. M. Warshaw, M. Periasamy, Smooth muscle myosin heavy chain isoforms and their role in muscle physiology. *Microsc. Res. Tech.* **50**, 532–540 (2000).
38. D. Wang, E. J. Bonten, G. Yogalingam, L. Mann, A. d'Azzo, Short-term, high dose enzyme replacement therapy in sialidosis mice. *Mol. Genet. Metab.* **85**, 181–189 (2005).
39. H. A. Cocker, C. R. Pinkerton, L. R. Kelland, Characterization and modulation of drug resistance of human paediatric rhabdomyosarcoma cell lines. *Br. J. Cancer* **83**, 338–345 (2000).
40. R. Kalluri, R. A. Weinberg, The basics of epithelial-mesenchymal transition. *J. Clin. Invest.* **119**, 1420–1428 (2009).
41. D. X. Nguyen, P. D. Bos, J. Massagué, Metastasis: From dissemination to organ-specific colonization. *Nat. Rev. Cancer* **9**, 274–284 (2009).
42. A. Arjonen, R. Kaukonen, E. Mattila, P. Rouhi, G. Högnäs, H. Sihto, B. W. Miller, J. P. Morton, E. Bucher, P. Taimen, R. Virtakoivu, Y. Cao, O. J. Sansom, H. Joensuu, J. Ivaska, Mutant p53-associated myosin-X upregulation promotes breast cancer invasion and metastasis. *J. Clin. Invest.* **124**, 1069–1082 (2014).
43. P. D. Bos, X. H. F. Zhang, C. Nadal, W. P. Shu, R. R. Gomis, D. X. Nguyen, A. J. Minn, M. J. van de Vijver, W. L. Gerald, J. A. Foekens, J. Massague, Genes that mediate breast cancer metastasis to the brain. *Nature* **459**, 1005–1009 (2009).
44. D. Schramek, A. Sendoel, J. P. Segal, S. Beronja, E. Heller, D. Oristian, B. Reva, E. Fuchs, Direct in vivo RNAi screen unveils myosin IIa as a tumor suppressor of squamous cell carcinomas. *Science* **343**, 309–313 (2014).
45. T. Miyagi, K. Yamaguchi, Mammalian sialidases: Physiological and pathological roles in cellular functions. *Glycobiology* **22**, 880–896 (2012).
46. A. Reddy, E. V. Caler, N. W. Andrews, Plasma membrane repair is mediated by Ca^{2+}-regulated exocytosis of lysosomes. *Cell* **106**, 157–169 (2001).
47. P. Saftig, J. Klumperman, Lysosome biogenesis and lysosomal membrane proteins: Trafficking meets function. *Nat. Rev. Mol. Cell Biol.* **10**, 623–635 (2009).
48. E. J. Blott, G. M. Griffiths, Secretory lysosomes. *Nat. Rev. Mol. Cell Biol.* **3**, 122–131 (2002).
49. E. Rainero, J. C. Norman, Late endosomal and lysosomal trafficking during integrin-mediated cell migration and invasion: Cell matrix receptors are trafficked through the late endosomal pathway in a way that dictates how cells migrate. *Bioessays* **35**, 523–532 (2013).
50. L. Lan, H. Han, H. Zuo, Z. Chen, Y. Du, W. Zhao, J. Gu, Z. Zhang, Upregulation of myosin Va by snail is involved in cancer cell migration and metastasis. *Int. J. Cancer* **126**, 53–64 (2010).
51. R. E. Palmer, S. B. Lee, J. C. Wong, P. A. Reynolds, H. Zhang, V. Truong, J. D. Oliner, W. L. Gerald, D. A. Haber, Induction of BAIAP3 by the EWS-WT1 chimeric fusion implicates regulated exocytosis in tumorigenesis. *Cancer Cell* **2**, 497–505 (2002).
52. A. Hendrix, D. Maynard, P. Pauwels, G. Braems, H. Denys, R. Van den Broecke, J. Lambert, S. Van Belle, V. Cocquyt, C. Gespach, M. Bracke, M. C. Seabra, W. A. Gahl, O. De Wever,

W. Westbroek, Effect of the secretory small GTPase Rab27B on breast cancer growth, invasion, and metastasis. *J. Natl. Cancer Inst.* **102**, 866–880 (2010).
53. H. M. Coley, Overcoming multidrug resistance in cancer: Clinical studies of P-glycoprotein inhibitors. *Methods Mol. Biol.* **596**, 341–358 (2010).
54. T. Yamagishi, S. Sahni, D. M. Sharp, A. Arvind, P. J. Jansson, D. R. Richardson, P-glycoprotein mediates drug resistance via a novel mechanism involving lysosomal sequestration. *J. Biol. Chem.* **288**, 31761–31771 (2013).
55. Y. Yagi, A. Machida, S. Toru, T. Kobayashi, T. Uchihara, Sialidosis type I with neoplasms in siblings: The first clinical cases. *Neurol. Sci.* **32**, 737–738 (2011).
56. T. Uchihara, K.-i. Ohashi, M. Kitagawa, M. Kurata, A. Nakamura, K. Hirokawa, T. Kasuga, T. Kobayashi, Sialidosis type I carrying V217M/G243R mutations in lysosomal sialidase: An autopsy study demonstrating terminal sialic acid in lysosomal lamellar inclusions and cerebellar dysplasia. *Acta Neuropathol.* **119**, 135–145 (2010).
57. H. Hanawa, P. F. Kelly, A. C. Nathwani, D. A. Persons, J. A. Vandergriff, P. Hargrove, E. F. Vanin, A. W. Nienhuis, Comparison of various envelope proteins for their ability to pseudotype lentiviral vectors and transduce primitive hematopoietic cells from human blood. *Mol. Ther.* **5**, 242–251 (2002).
58. E. J. Bonten, D. Wang, J. N. Toy, L. Mann, A. Mignardot, G. Yogalingam, A. d'Azzo, Targeting macrophages with baculovirus-produced lysosomal enzymes: Implications for enzyme replacement therapy of the glycoprotein storage disorder galactosialidosis. *FASEB J.* **18**, 971–973 (2004).
59. D. Axelrod, Cell-substrate contacts illuminated by total internal reflection fluorescence. *J. Cell Biol.* **89**, 141–145 (1981).
60. R. J. Simpson, H. Kalra, S. Mathivanan, ExoCarta as a resource for exosomal research. *J. Extracell. Vesicles* **1**, 18374 (2012).
61. A. D. Marshall, I. Lagutina, G. C. Grosveld, PAX3-FOXO1 induces cannabinoid receptor 1 to enhance cell invasion and metastasis. *Cancer Res.* **71**, 7471–7480 (2011).

Acknowledgments: We thank G. Grosveld, D. Green, M. Hatley, J. Opferman, L. Zhu, K. Freeman, and B. Sosa-Pineda for critical reading of the manuscript and insightful suggestions; H. Hu for some immunohistochemistry; F. Harwood for help with the culture of primary sarcoma cells; the VPC staff for performing human tissue and animal necropsies; C. Calabrese and the Small Animal Imaging Center staff for bioluminescence imaging; J. Rehg for help with histopathology; and E. Schuetz for the anti-PgP antibody. **Funding:** A.d'A. holds the Jewelers for Children Endowed Chair in Genetics and Gene Therapy. This work was funded, in part, by NIH grants GM60905, DK52025, CA021764, and GM104981; CCSG St. Jude Developmental Funds, and American Lebanese Syrian Associated Charities. **Author contributions:** A.d'A. conceived the project and designed and supervised the research. E.M., S.W.-G., and A.d'A. wrote the manuscript. E.M., S.W.-G., D.v.d.V., S.M., Y.C., R.M., X.Q., and I.A. designed, performed, and analyzed experiments. L.J. performed the pathology. D.F. analyzed the gene expression data. E.G. maintained the animal colonies and generated xenografts. C.L.M. performed and provided the human RMS xenografts. **Competing interests:** A.d'A., S.W.-G., and I.A. are named as co-inventors on patent application 61/544,855, which is based, in part, on the research reported herein. The other authors declare that they have no competing interests. **Data and materials availability:** All data needed to evaluate the conclusions in the paper are present in the paper and/or the Supplementary Materials. Additional data related to this paper may be requested from the authors.

Submitted 14 May 2015
Accepted 29 September 2015
Published 18 December 2015
10.1126/sciadv.1500603

Citation: E. Machado, S. White-Gilbertson, D. van de Vlekkert, L. Janke, S. Moshiach, Y. Campos, D. Finkelstein, E. Gomero, R. Mosca, X. Qiu, C. L. Morton, I. Annunziata, A. d'Azzo, Regulated lysosomal exocytosis mediates cancer progression. *Sci. Adv.* **1**, e1500603 (2015).